EBioMedicine 45 (2019) 393–407

Contents lists available at ScienceDirect

EBioMedicine

journal homepage: www.ebiomedicine.com

EBioMedicine
Published by THE LANCET

Research paper

Paricalcitol accelerates BACE1 lysosomal degradation and inhibits calpain-1 dependent neuronal loss in APP/PS1 transgenic mice

Yong-Gang Fan [a], Tian Guo [a], Xiao-Ran Han [a], Jun-Lin Liu [a], Yu-Ting Cai [a], Han Xue [a], Xue-Shi Huang [a], Yan-Chun Li [b], Zhan-You Wang [a,c,*], Chuang Guo [a,*]

[a] College of Life and Health Sciences, Northeastern University, NO.195, Chuangxin Road, Hunnan District, Shenyang 110169, China
[b] Department of Medicine, the University of Chicago, Chicago, IL 60637, USA
[c] Institute of Health Sciences, Key Laboratory of Medical Cell Biology of Ministry of Education, China Medical University, Shenyang 110122, China

ARTICLE INFO

Article history:
Received 6 May 2019
Received in revised form 1 July 2019
Accepted 4 July 2019
Available online 11 July 2019

Keywords:
Alzheimer's disease
Paricalcitol
β-Site APP cleavage enzyme 1
8-hydroxyguanosine
Lysosomal degradation
Neuronal loss

ABSTRACT

Background: Recent studies have revealed that vitamin D deficiency may increase the risk of Alzheimer's disease, and vitamin D supplementation may be effective strategy to ameliorate the neurodegenerative process in Alzheimer's disease patients. Paricalcitol (PAL), a low-calcemic vitamin D receptor agonist, is clinically used to treat secondary hyperparathyroidism. However, the potential application of PAL for treating neurodegenerative disorders remains unexplored.
Methods: The APP/PS1 mice were intraperitoneally injected with PAL or vehicle every other day for 15 weeks. The β-amyloid (Aβ) production was confirmed using immunostaining and enzyme linked immunosorbent assay. The underlying mechanism was verified by western blot and immunostaining in vivo and in vitro.
Findings: Long-term PAL treatment clearly reduced β-amyloid (Aβ) generation and neuronal loss in APP/PS1 transgenic mouse brains. PAL stimulated the expression of low-density lipoprotein receptor-related protein 1 (LRP1) possibly through inhibiting sterol regulatory element binding protein-2 (SREBP2); PAL also promoted LRP1-mediated β-site APP cleavage enzyme 1 (BACE1) transport to late endosomes, thus increasing the lysosomal degradation of BACE1. Furthermore, PAL diminished 8-hydroxyguanosine (8-OHdG) generation in neuronal mitochondria via enhancing base excision repair (BER), resulting in the attenuation of calpain-1-mediated neuronal loss.
Interpretation: The present data demonstrate that PAL can reduce Aβ generation through accelerating BACE1 lysosomal degradation and can inhibit neuronal loss through suppressing mitochondrial 8-OHdG generation. Hence, PAL might be a promising agent for treating Alzheimer's disease.
Fund: This study was financially supported by the Natural Science Foundation of China (U1608282).

1. Introduction

Vitamin D deficiency receives considerable attention worldwide, and interest in vitamin D has been renewed because of its contributions to the development of many neurological diseases, including Alzheimer' disease [1,2]. Multiple epidemiologic studies suggested that vitamin D deficiency might be associated with cognitive impairment in both Alzheimer's disease patients and the general population [2,3]. Growing clinical evidence revealed that vitamin D supplementation could effectively ameliorate the neurodegenerative process in Alzheimer's disease patients [4,5]. Very recently, an interventional study revealed that vitamin D may increase the serum levels of the amyloid-β (Aβ) peptide Aβ40 in Alzheimer's disease patients, suggesting improved Aβ clearance [6]. Consistently, Durk et al. [7] reported that the long-term administration of vitamin D to TgCRND8 mice reduced the soluble and insoluble Aβ load, which led to improvements in conditioned fear memory. However, the data from vitamin D intervention studies are inconclusive regarding cognitive performance in healthy older adults and Alzheimer's disease patients [3]; these shortcomings have helped produce well-designed interventions, but much effort is still directed towards exploring new strategies.

Paricalcitol (PAL) is a low-calcemic vitamin D analogue widely used for treating secondary hyperparathyroidism in chronic kidney diseases. As a vitamin D receptor (VDR) agonist, PAL has powerful anti-inflammatory and anti-oxidative capacities and is used to prevent ischaemia/reperfusion injury and seizures [8,9]. Although animal and cell culture evidence show that vitamin D supplementation may diminish the amyloid-β (Aβ) burden and increase Aβ clearance [7,10–12], the potential role of PAL in amyloid

* Corresponding authors at: College of Life and Health Sciences, Northeastern University, NO.195, Chuangxin Road, Hunnan District, Shenyang 110169, China.
E-mail addresses: wangzy@mail.neu.edu.cn (Z.-Y. Wang), guoc@mail.neu.edu.cn (C. Guo).

https://doi.org/10.1016/j.ebiom.2019.07.014

Research in context

Evidence before this study

Vitamin D receptor (VDR) signaling may be a potential target for the treatment of Alzheimer's disease. β-site APP cleavage enzyme 1 (BACE1) is the rate-limiting step in the production of β-amyloid (Aβ), it can be downregulated by low-density lipoprotein receptor-related protein 1 (LRP1) through promoting its lysosomal degradation; LRP1 expression was elevated after vitamin D supplementation in mouse brains, these studies suggested that Aβ generation may be regulated by VDR signaling. Moreover, 8-Oxoguanine (8-oxoG) was robustly generated in the brains of Alzheimer's disease patients and animals. Recent studies uncovered that 8-oxoG accumulation induces calpain-1-mediated cell death under oxidative conditions. Since calpian-1 expression can be influenced by VDR, we proposed that VDR signaling may regulate neuronal death via targeting 8-oxoG production in the pathology of Alzheimer's disease.

Added value of study

Paricalcitol (PAL), a low-calcemic vitamin D receptor agonist, is clinically used to treat secondary hyperparathyroidism. In this study, we identified the potential functions of PAL in APP/PS1 mice. We found that PAL promotes LRP1-mediated BACE1 transport to late endosomes, thus increasing the lysosomal degradation of BACE1 in APP/PS1 mouse brains. Furthermore, PAL diminished 8-OHdG generation in neuronal mitochondria via enhancing base excision repair (BER), resulting in the attenuation of calpain-1-mediated neuronal loss in APP/PS1 mouse brains.

Implications of all the available evidence

PAL treatment obviously improved the cognitive abilities of APP/PS1 mice via decreasing Aβ production and reducing neuronal death. PAL's status as a clinical drug used for the treatment of secondary hyperparathyroidism has an added advantage of being readily repurposed for treating the patients with Alzheimer's disease.

pathology has not been examined in any animal models of Alzheimer's disease. As is well known, amyloid precursor protein (APP) processing by β-site APP cleavage enzyme 1 (BACE1) and γ-secretase is the predominant mechanism of Aβ generation [13,14]. Of course, APP can also be cleaved into sAPPα and αCTF via α-secretase, which constitutes a non-amyloidogenic pathway [15]. Mounting evidence has shown that BACE1 is the rate-limiting step in the production of Aβ [13,16]. Targeting BACE1 can effectively suppress Aβ generation, indicated by improved cognitive and memory capacities in several animal models of Alzheimer's disease [17,18]. Interestingly, it has been reported that several vitamin D analogues decrease Aβ formation and increase Aβ degradation in vitamin D deficient mouse brains or neuroblastoma cells [19]. However, the exact underlying mechanisms remain to be elucidated.

BACE1 is a single membrane-spanning protease synthesized in the endoplasmic reticulum and delivered to the cell surface from the trans-Golgi network (TGN). Mature BACE1 is internalized from the plasma membrane or directly from the TGN into endosomes [20,21] where a sealed acid environment is critical for the amyloidogenic processing of APP by BACE1 [20,22]; BACE1 is subsequently submitted to lysosomal degradation [23,24]. BACE1 was significantly increased in hAPP transgenic (Tg) mice due to impaired late endocytic trafficking, rather than upregulated transcriptional expression [24]. It was reported that Snapin overexpression induced BACE1 retrograde transport and turnover through lysosomes in the neurons and thereby reduced BACE1-mediated Aβ production [24,25]. Low-density lipoprotein receptor-related protein 1 (LRP1) is widely accepted to play an active role in transporting Aβ across the blood-brain barrier [26,27]. Notably, LRP1 was recently demonstrated to reduce the protein stability and cell-surface expression of BACE1 via protein-protein interactions, which promote the lysosomal degradation of BACE1 [28]. Based on these observations, targeting LRP1 may not only enhance the brain efflux of Aβ but also reduce BACE1 expression by improving BACE1 retrograde transport. In addition, inhibiting SREBP2, the only known transcription repressor of LRP1, effectively reduced Aβ burden in APP/PS1 mice [29]. SREBP activation can be suppressed by sterols due to a feedback mechanism [30]. Furthermore, Vitamin D treatment or VDR activation decreases SREBP expression in the kidney [31]. These results prompted us to investigate whether PAL can be used as a therapeutic agent for Alzheimer's disease and the exact molecular mechanisms that might be involved in SREBP2/LRP1/BACE1 singling.

In addition to BACE1, it has recently been demonstrated that VDRs are colocalized with APP and/or secretase complexes on the neuronal plasma membrane [32], and Aβ triggers neurodegeneration by dramatically suppressing VDR expression [33]. More importantly, vitamin D deficiency in early life affects neuronal differentiation, axonal connectivity, dopamine ontogeny and brain structure and function [34], but vitamin D supplementation protects neurons by preventing cytotoxicity and apoptosis and by upregulating VDR expression [7,33]. Indeed, elevated levels of Aβ have been associated with increased levels of protein, lipid and nucleic acid oxidation products in the hippocampus and cortex in Alzheimer's disease [35]. 8-Oxoguanine (8-oxoG), a major form of oxidized base lesions, can be caused directly by guanine in DNA or by the integration of 8-hydroxyguanosine (8-OHdG) into DNA from nucleotide pools under oxidative conditions. The incorporation of 8-oxoG into nascent strands leads to improper pairing with adenine and induces G:C to A:T transversion mutations [36]. MTH1, OGG1 and MUTYH are the three main enzymes responsible for directing against 8-oxoG to prevent spontaneous mutations. Previous studies show that an increased number of mtDNA mutations with age promoted Aβ accumulation and brain atrophy in a mouse model of Alzheimer's disease [37]. Furthermore, mtDNA mutations are abundant in the mitochondria of Alzheimer's disease patients; these mutations are highly correlated with base excision repair (BER) deficiency [38]. Although 8-oxoG is robustly generated in postmortem Alzheimer's disease brains [39], the function of 8-oxoG remains unclear as it is usually recognized as an indicator of oxidative stress damage. Recently, reports from Nakabeppu's group demonstrated that 8-oxoG accumulation in mtDNA triggered mitochondrial dysfunction and impaired neuritogenesis in mouse cortical neurons in vitro [40,41]. Further studies revealed that 8-oxoG accumulates predominantly in the neuronal mtDNA of mice lacking OGG1 and/or MTH1 under oxidative conditions, thus leading to calpain-dependent neuronal death [42]. These observations suggest that targeting 8-oxoG could be a reliable strategy for preventing cell death in neurodegenerative disease. Thus, questions arise regarding whether PAL treatment influences Aβ-induced 8-oxoG accumulation and neuronal death, which are involved in Alzheimer's disease pathogenesis and progression.

In this study, we investigated the effects of PAL on Aβ metabolism and neuronal loss in APP/PS1 transgenic mice. We first demonstrated that long-term treatment with PAL improved the cognitive ability of APP/PS1 mice by decreasing Aβ production, senile plaque (SP) burden and neuronal loss.

2. Materials and methods

2.1. Reagents

Paricalcitol (19-nor-1, 25-dihydroxyvitamin D2, PAL) was purchased from Sigma-Aldrich (1499403), which was dissolved in 60%

propylene glycol for stock solution and stored at −80 °C. For the injection of PAL, the stock solution was further diluted by physiological saline.

2.2. Animal treatment

The APPswe/PSEN1dE9 (APP/PS1) transgenic mice, a C57BL6 strain of mice with human APPSwe and PS1-dE9 mutations, were purchased from the Jackson Laboratory. The animals were maintained in cages in a controlled environment with free access to standard diet and distilled water. A total of twenty female APP/PS1 mice at the age of 6-month-old were randomly divided into two treatment groups: vehicle-treated group and PAL-treated group. Mice were intraperitoneally injected with PAL (200 ng/kg) or vehicle once every two days for 15 weeks as our previous report [43]. This study was carried out in accordance with the recommendations of "Laboratory Animals-Guideline of welfare and ethics, The Ethics Committee for Medical Laboratory Animals of China Medical University". The protocol was approved by The Ethics Committee for Medical Laboratory Animals of China Medical University.

2.3. Tissue preparation

Twenty-four hours after the last intraperitoneally injected with PAL or vehicle, mice were anesthetized with sodium pentobarbital (50 mg/kg, intraperitoneally). Mice were subsequently transcardially perfused with physiological saline and sacrificed by decapitation. Brains were immediately removed and dissected in half on an ice-cold board. One was fixed in the 4% polyformaldehyde for morphological assessment, the other half was frozen at −80 °C for biochemical analyses.

2.4. Aβ42 oligomer preparation

The Aβ42 oligomer was generated as previously described [44,45]. Briefly, the lyophilized Aβ42 peptide (ChinaPeptides, China) was dissolved in 1,1,1,3,3,3-hexafluoro-2-propanol (HFIP; Sigma) and divided into quarters before removing HFIP. The Aβ42 oligomer was obtained through incubating in 4 °C for 24 h in F12 medium. The quality of the Aβ42 oligomer was controlled with Western blotting using the antibody against Aβ oligomer (Millipore, AB9234, 1: 1000).

2.5. Cell culture and treatment

The N2a-sw cells and N2a cells were a gift from Professor Huaxi Xu in Xiamen University. The N2a-sw cells (passage 5–11) and N2a cells (passage 28–33) were used for the in vitro studies. Cells were cultured in high glucose DMEM (Gibco, Carlsbad, CA) containing 10% FBS (Gibco, Carlsbad, CA), 100 U/mL penicillin (Sigma), 100 μg/mL streptomycin (Sigma) at 37 °C in a humidified atmosphere of 5% CO_2. Cells were seed onto six-well plate or slides for 36 h and subsequently starved in FBS free medium for 12 h before PAL (0–30 nM) and/or Aβ42 oligomer (2 μM) treatment for 24 h. Cells were harvested and analysed.

2.6. Cell viability analysis

Cells were seeded in 96 well plates until 70% confluence. The gradient concentrations of PAL (0–30 nM) were added to the N2a-sw cells and subsequently incubated for 24 h. The N2a cells were pretreated with PAL (15 nM) for 4 h or calpain-1 inhibitor MDL-28170 (5 μM) for 1 h and subsequently treated with PAL (15 nM) and/or Aβ42 oligomer (2 μM) for 24 h. Then cells were coincubated with 20 μL [3-(4,5-dimethylthiazol-2-yl)-2,5-diphenyltetrazolium bromide] (MTT; Sigma) for 4 h. The media were discarded and 150 μL DMSO were added in each well. The absorbance of each well solution was recorded using a microplate reader (Themo Fisher Scientific, 1510) at wavelength of 490 nm. The percentage of cell viability relative to vehicle group was calculated. Experiments were repeated at least three times in quadruplicate.

2.7. Trypan blue exclusion assay

The N2a cells were pretreated with PAL (15 nM) for 4 h or calpain-1 inhibitor MDL-28170 (5 μM) for 1 h. Cells were subsequently treated with PAL (15 nM) and/or Aβ42 oligomer (2 μM) for 24 h. Cells were harvested and incubated with 0.04% trypan blue for 5 min at room temperature. Trypan blue only stains the dead cells. After washing with PBS, cells were resuspended in PBS and the living and dead cells were counted. The death rate (%) = number of dead cells / (number of living cells + number of dead cells) × 100.

2.8. Real-time PCR

The total RNA was isolated from cerebral cortex tissues or N2a-sw cells using TRIzol reagents (Invitrogen, 15,596,026) according to the manufacturer's instructions. One microgram of total RNA was reverse transcribed to cDNA using GoTaqR 2-Step RT-qPCR System (Promega, A5001) and the cDNA obtained was used for subsequent PCR reactions. All PCR reactions performed in a total volume of 20 μL: DNA polymerase activation at 95 °C for 10 min, and 40 cycles of denaturing at 95 °C for 30 s and annealing and extension at 58 °C for 30 s. The following PCR primers were used: BACE1: forward, GCATGATCATTGGTGGTATC and reverse, CCATCTTGAGATCTTGACCA; APP: forward, GGATGCAGAGG AGGATGACT and reverse, CTCCTCTTCGGCGACTTCTA; LRP1: forward, CGAGGAGCAGGTTGTTAG and reverse, CAGAAGCAGCAGGAGAAG; GAPDH: forward, GCCTTCCGTGTTCCTACC and reverse, AGAGTGGGA GTTGCTGTTG. The mRNA expression was calculated using ΔΔCt (threshold cycle, Ct) values normalized to GAPDH.

2.9. Immunostaining

Brains from the six-month-old mice treated with PAL or vehicle for 15 weeks were collected and cut on a cryostat (Leica, CM1850) at a thickness of 10 μm. A series of three equally spaced brain sections (~1 mm apart) were used for each type of stain. The slides or cells were fixed with 4% paraformaldehyde for 10 min and subsequently permeabilized with 0.2% Triton X-100 for 5 min at room temperature. After blockage with 5% BSA (sigma-Aldrich) for 1 h, sections or cells were incubated with mouse anti-VDR (Santa Cruz, sc-13,133, 1: 50), mouse anti-Aβ (Santa Cruz sc-28,365, 1: 400), mouse anti-BACE1 (Santa Cruz, sc-33,711, 1: 50), rabbit anti-LRP1 (Abcam, ab92544, 1: 100), rabbit anti-NeuN (Cell Signaling Technology, 12,943 s, 1: 200), mouse anti-cathepsin D (Santa Cruz, sc-377,299, 1:20), goat anti-rab7a (Biorbyt, orb180471, 1:50), rabbit anti-LAMP1 (Abcam, ab24170, 1: 100), rabbit anti-GFAP (Abcam, ab7260, 1: 200), rabbit anti-Iba1 (Abcam, ab153696, 1: 200) overnight at 4 °C. The secondary antibodies, goat anti-mouse-Ig G Alexa 488 (Themo Fisher Scientific, A32723, 1:300), goat anti-rabbit-Ig G Alexa 555 (Themo Fisher Scientific, A32732, 1:300), rabbit anti-goat-IgG Alexa 555 (Themo Fisher Scientific, A27017, 1:300) were used. Images of half mouse brains from Aβ staining were captured by fluorescent microscope (Nikon, NI-SH-E), the numbers and areas of Aβ-positive plaques were quantified using Image J software. The other images were obtained using a confocal laser microscope (Leica, SP8) and the fluorescent intensities were quantified using Image J or Image-Pro Plus software.

For quantitative immunodetection of 8-OHdG in mtDNA, sections were pretreated as previous reports [42]. Briefly, after treatment of Triton X-100, sections were incubated with RNase A (5 mg/mL; Sigma) at 37 °C for 1 h and subsequently denaturation with ice 25 mM NaOH in 50% ethanol. Then, sections were incubated with mouse anti-8-OHdG (Abcam, ab62623, 1: 100) and rabbit anti-NeuN (Cell Signaling Technology, 12,943 s, 1: 200), and the following steps were described above. Images were obtained using a confocal laser microscope (Leica, SP8).

At least twenty neurons for each section were measured using Image J software to evaluate the mitochondrial 8-OHdG index in a single neuron in cortex [42].

2.10. Immunohistochemistry

Paraffin-embedded brains were sectioned at a thickness of 5 μm. A series of three equally spaced brain sections (~1 mm apart) were used for this experiment. Sections were then dewaxed and followed by antigen retrieval using L.A.B solution (Polyscience, Inc) for 20 min. After the blockage of goat serum for 30 min, the sections were incubated with rabbit anti-NeuN (Cell Signaling Technology, 12,943 s, 1: 200) and mouse anti-synaptophysin (SYP; Santa Cruz, sc-365,488, 1:50) overnight at 4 °C. Next, sections were treated with appropriate secondary antibodies for 1 h and third antibody for 30 min at room temperature, and subsequently developed in DAB for 3 min. Finally, the sections were dehydrated and sealed. The images of half mouse brains were obtained from a light microscope (Leica, DM4000B). The NeuN positive cells in cortexes and SYP intensities in CA1 regions and cortexes were quantified using Image J software. For the quantification of SYP in CA1 regions, a rectangle spanning 200 μm was drawn over CA1 in Image J, the same size rectangle was used for each section. The numbers of NueN positive cells in cortexes and intensities of SYP in cortexes and CA1 regions were averaged to generate a single value per mouse.

2.11. Sandwich ELISA

For the detection of Aβ, the cortex and hippocampus from vehicle control- or PAL-treated APP/PS1 transgenic mice were weighed and subsequently homogenized in 20 mM Tris buffer (pH 8.5) for soluble Aβ or in 5 M guanidine HCl/50 mM Tris-HCl (pH 8.0) for insoluble Aβ as our previously described [18]. The homogenates were centrifuged for 30 min at 4 °C, and the supernatants were diluted with dilution buffer at an appropriate ratio. The mixtures were then immediately added to 96-well plates. Aβ40 and Aβ42 level were respectively determined using Aβ40 kits (Invitrogen, KHB3481) and Aβ42 kits (Invitrogen, HKB3544) according to the manufacturer's instructions. Absorbance values were recorded using a microplate reader at a wavelength of 450 nm.

2.12. Western blot

Cortexes or cells were lysed with lysis buffer and proteins were quantified using microplate reader at wavelength of 560 nm. Nuclear proteins were isolated using nucleoprotein extraction kit (Sangon Biotech, BSP009) according to manufacturer's instructions. Equal proteins were subjected to SDS/PAGE to separate, the proteins were transferred to PVDF membranes and incubated with mouse anti-VDR (Santa Cruz, sc-13,133, 1: 500), rabbit anti-BACE1 (Abcam, ab183612, 1: 1000), rabbit anti-APP695 (Cell Signaling Technology, 2452, 1: 1000), rabbit anti-C-APP (Sigma, SAB4200535, 1:1000), rabbit anti-PS1 (Cell Signaling Technology, 5643, 1: 1000), rabbit anti-AMAD 10 (Cell Signaling Technology, 14,194, 1: 1000), mouse anti-soluble amyloid precursor α (sAPPα; Immuno-Biological Laboratories, 11,088, 1: 500), mouse anti-soluble amyloid precursor β (sAPPβ; Immuno-Biological Laboratories, 10,321, 1: 500), rabbit anti-advanced glycation end products (RAGE; Sigma, SAB2105049, 1: 1000), goat anti-apolipoprotein (APOE; Santa Cruz, sc-6384, 1: 500), mouse anti-LRP1 (Santa Cruz, sc-57,353, 1: 400), rabbit anti-LRP1 (Abcam, ab92544, 1: 8000), mouse anti-insulin-degrading enzyme (IDE; Santa Cruz, sc-514,458, 1:500), mouse anti-neprilysin (NEP; Santa Cruz, sc-46,656, 1: 500), mouse anti-HSP70 (Themo Fisher Scientific, MA3–008, 1: 2000), rabbit anti-Rab5c (Themo Fisher Scientific, PA5–36606, 1: 500), goat anti-Rab7a (Biorbyt, orb180471, 1: 1000), rabbit anti-postsynaptic density proteins 95 (PSD95; Cell Signaling Technology, 3409, 1: 2000), mouse anti-synaptophysin (SYP; Santa Cruz, sc-365,488, 1:1000), mouse anti-OGG1 (Santa Cruz, sc-376,935, 1: 500), mouse anti-MTH1 (Santa Cruz, sc-271,082, 1: 500), mouse anti-MUTYH (Santa Cruz, sc-374,571, 1: 500), rabbit anti-LAMP1 (Abcam, ab24170, 1: 1000), rabbit anti-LAMP2 (Abcam, ab18528, 1: 1000), rabbit anti-NeuN (Cell Signaling Technology, 12,943 s, 1: 2000), rabbit anti-IL-1β (Santa Cruz, sc-7884, 1: 500) or mouse anti-TNFα (Santa Cruz, sc-52,746, 1: 500) overnight at 4 °C. For the detection of Aβ Oligomer 56, the rabbit anti-Oligomer (Millipore, AB9234, 1: 1000) was employed and the experimental procedures were performed as previous reports [46,47]. Briefly, the cortexes were dissociated in the cold NP40-lysis buffer and centrifuged at 800 *g* for 10 min at 4 °C. The supernatants were collected and further centrifuged at 16100 *g* for 90 min at 4 °C, this step was performed once again, and the supernatants were the extracellular-enriched fractions which were used for the further detection of Aβ Oligomer 56. The collected supernatants were further immunodepleted before the protein concentration was assessed. The supernatants were mixed with 4× tricine loading buffer with β-mercaptoethanol (βME) and Tris-Tricine gels were used for the further analysis. Membranes were washed with TBST and subsequently incubated with horseradish peroxidase (HRP)-labeled secondary antibodies for 1 h at room temperature. Enhanced chemiluminescence (ECL) kits (Tanon, 180–5001) and Chem Doc XRS with Quantity One software (Bio-Rad, 5500) were applied to detect blots. Data from the bands were determined using Image J software.

2.13. Morris water maze

After 15 weeks of treatment with PAL, mice were trained for 2 days and then tested for 5 days using a Morris water maze. The MWM apparatus comprise of a circular water tank (100 cm dia. x 40 cm H) and a platform (5 cm dia.). The water (22 ± 1 °C, 26 cm H) was rendered opaque through addition of the nontoxic, water-soluble white ink. Briefly, the mice were subjected to pre-training (visible platform), composed of 5 trials with intervals of 30 min over 2 days. A limit of 1 min was given for the mice to find the visible platform. The platform was then placed opposite to the location used in the visible platform task and submerged 1 cm below the water surface. The animals performed 5 trials per day and the releasing locations were selected randomly from each of five indicated positions. The escape latency and the path length before the mice found the hidden platform were recorded to evaluate their spatial learning scores. On the last day, the platform was removed, and the number of times that the mice crossed the platform region was recorded for 1 min. Finally, the recorded data were analysed with a computer program (Panlab, SMART 3.0).

2.14. Nest construction

The nest construction test was employed to assess the social behavior of mice and the detail procedures and related scores were introduced as previously [48].

2.15. Statistical analysis

All the experiments and analyses are conducted with the experimenter blind to drug treatment. All values are presented as the mean ± SEM. Statistical significances between the PAL treatment group and the vehicle control treatment group were determined by *t*-test or one-way analysis of variance (ANOVA). A critical value for significance of $p < .05$ was used throughout this study.

3. Results

3.1. PAL treatment improves the cognitive capacity of APP/PS1 mice

The Fig. 1a is the schematic drawing of the time course in this study. The Morris water maze test was performed to evaluate the spatial

learning and memory abilities of mice. In the visible platform test, we did not find significant differences between the PAL (chemical structure shown in Fig. 1g) treatment and vehicle control groups for escape latency (Fig. 1b) or path length (Fig. 1c), indicating that PAL treatment did not affect vision and motility in this animal model. However, in the hidden platform tests, PAL-treated mice spent less time (Fig. 1d) and travelled shorter lengths (Fig. 1e) when searching for the hidden platform than vehicle control-treated mice. Since the significant reductions in the escape latency and path length were observed on day 3 in PAL-treated group compared to vehicle-treated group, and the escape latency and path length remained unchanged in the hidden platform tests in PAL-treated group, we therefore evaluated the escape latency and path length on the first trial of day 3. The escape latency and path length on the first trial of day 3 were not significantly changed (Supplementary Fig. 1), suggesting that PAL treatment could improve the cognitive ability of APP/PS1. Moreover, the probe trial performed on the last day of the testing indicated a significant increase in the passing times of the PAL treatment group compared to those of the vehicle control group (Fig. 1f; vehicle = 2.9 ± 0.3 vs PAL = 4.6 ± 0.7), further suggesting that the cognitive capacity of APP/PS1 mice was improved after PAL

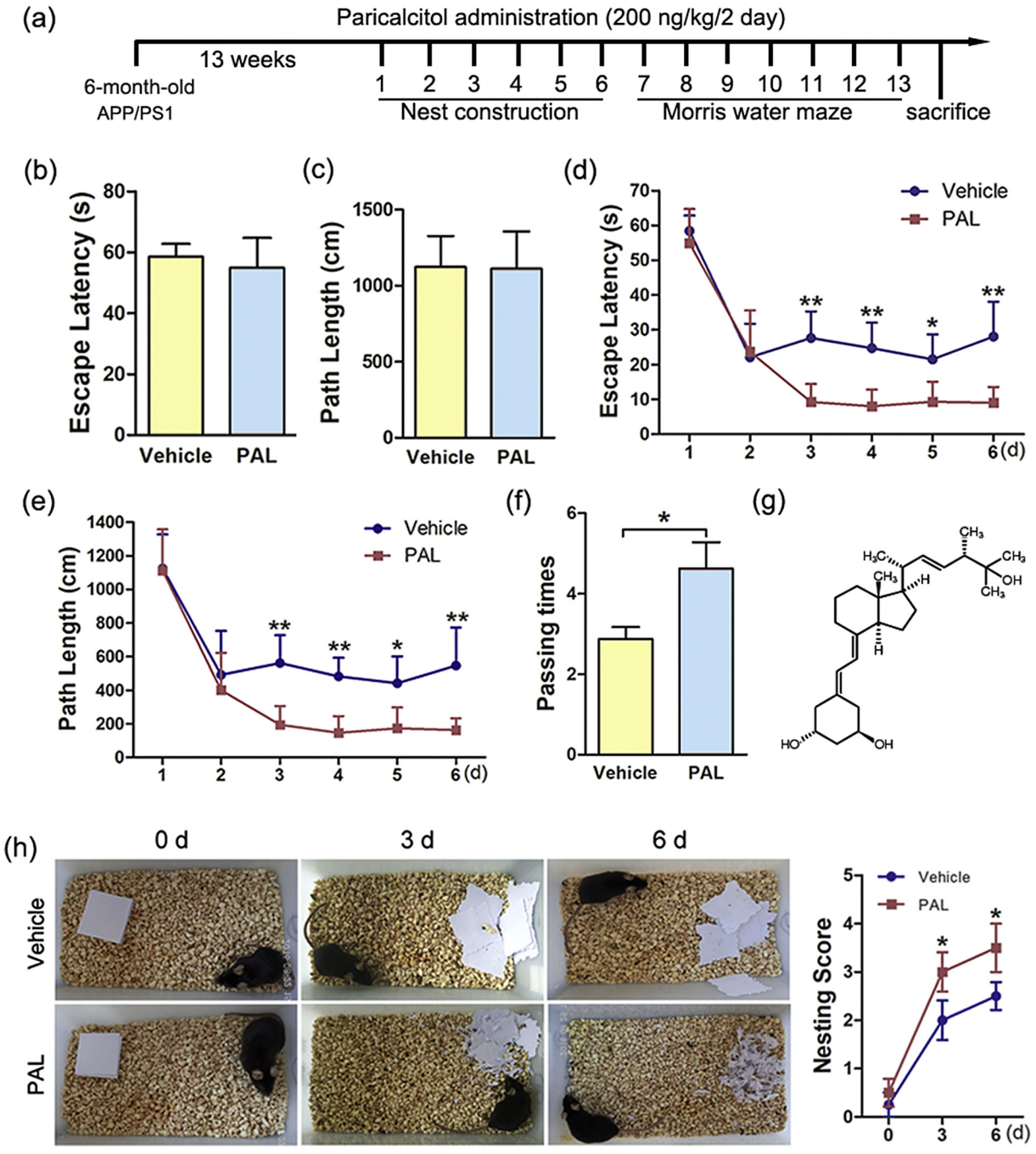

Fig. 1. PAL treatment improves the cognitive capacity of APP/PS1 mice. APP/PS1 mice that were six-months-old were treated with PAL (i.p., 200 ng/kg/2 d) for 14 weeks. Morris water maze tests with 2 days of visible platform training, 4 days of hidden platform testing and a probe trial after 24 h of the last hidden platform test were used to evaluate cognitive ability. (a) The schematic drawing of the time course in this study. (b-c) Mice from different groups exhibited a similar escape latency and path length to the visible platform at day 1. (d-e) The hidden platform tests showed that PAL treatment obviously decreased both the escape latency and path length from the 3rd day to the 6th day. (f) In the probe trial, PAL treatment significantly increased the time spent crossing the platform's former location. Nest construction was visualized after 13 weeks of PAL treatment. (g) The chemical structure of PAL. (h) PAL treatment significant rescued the impaired ability to construct nests. $n = 10$. $^{*}p < .05$, $^{**}p < .01$ (Student's-*t*-test).

treatment. Nest construction is an inherited social behaviour for mice, and this ability can be gradually impaired in APP/PS1 mice. Following PAL treatment, this impairment was largely rescued in APP/PS1 mice compared with that in control mice (Fig. 1h).

3.2. PAL treatment reduces Aβ generation in APP/PS1 mice

At the end of treatment, the mice were sacrificed, and Aβ plaque was visualized using immunofluorescence (Fig. 2a). PAL treatment caused a ~30% reduction in the number of Aβ plaque and a ~50% reduction in the area of Aβ plaque (Fig. 2b, c) in the cortex of APP/PS1 mice. Although we did not find a significant decrease in the number of Aβ plaque in the hippocampus (Fig. 2b), the area of Aβ plaque was reduced to ~65% after PAL treatment (Fig. 2c). Immunoblotting assays also detected a ~35% reduction in Aβ oligomer contents after PAL treatment (Fig. 2d). The Aβ40 and Aβ42 concentrations in the cortex and hippocampus were assessed using sandwich ELISAs. As shown in Fig. 2e, h, the soluble and insoluble Aβ40 levels in the hippocampus were slightly but significantly lower (Fig. 2e; vehicle = 10.2 ± 2.3 vs PAL = 7.5 ± 1.6. Fig. 2h; vehicle = 942.3 ± 183.8 vs PAL = 611.3 ± 244.1) in the PAL treatment group than in the vehicle control group; interestingly, the soluble and insoluble Aβ42 levels were considerably reduced in both the cortex (Fig. 2f; vehicle = 15.8 ± 1.5 vs PAL = 7.8 ± 0.3. Fig. 2i; vehicle = 1315.3 ± 201.4 vs PAL = 749.3 ± 125.7) and hippocampus (Fig. 2f; vehicle = 32.9 ± 3.5 vs PAL = 13.9 ± 1.6. Fig. 2i; vehicle = 2838.3 ± 157.1 vs PAL = 1238.1 ± 149.6) in the PAL treatment group. Furthermore, the ratios of soluble Aβ42/Aβ40 were also decreased in the cortex (Fig. 2g; vehicle = 2.7 ± 0.5 vs PAL = 1.5 ± 0.2) and the ratios of soluble and insoluble Aβ42/Aβ40 were both decreased in the hippocampus (Fig. 2 g; vehicle = 3.2 ± 0.4 vs PAL = 1.9 ± 0.2. Fig. 2j; vehicle = 3.1 ± 0.4 vs PAL = 2.0 ± 0.2) in the PAL treatment group. Immunoblotting results also showed a significant reduction in Aβ generation in PAL-treated mice compared to vehicle-treated mice (Supplementary Fig. 2).

3.3. PAL treatment decreases BACE1 expression in APP/PS1 mice

Immunostaining showed that VDR expression was mostly restricted to NeuN (a post-mitotic neuronal marker)-positive cells (Fig. 3a), the endothelium (Fig. 3a, large arrows) and glial cells (Fig. 3a, small arrows), and PAL treatment increased VDR expression by ~35% (Fig. 3b). Because SREBP2 is regulated by VDR [30,31], we then analysed the expression of SREBP2. As expected, total SREBP2 expression was reduced

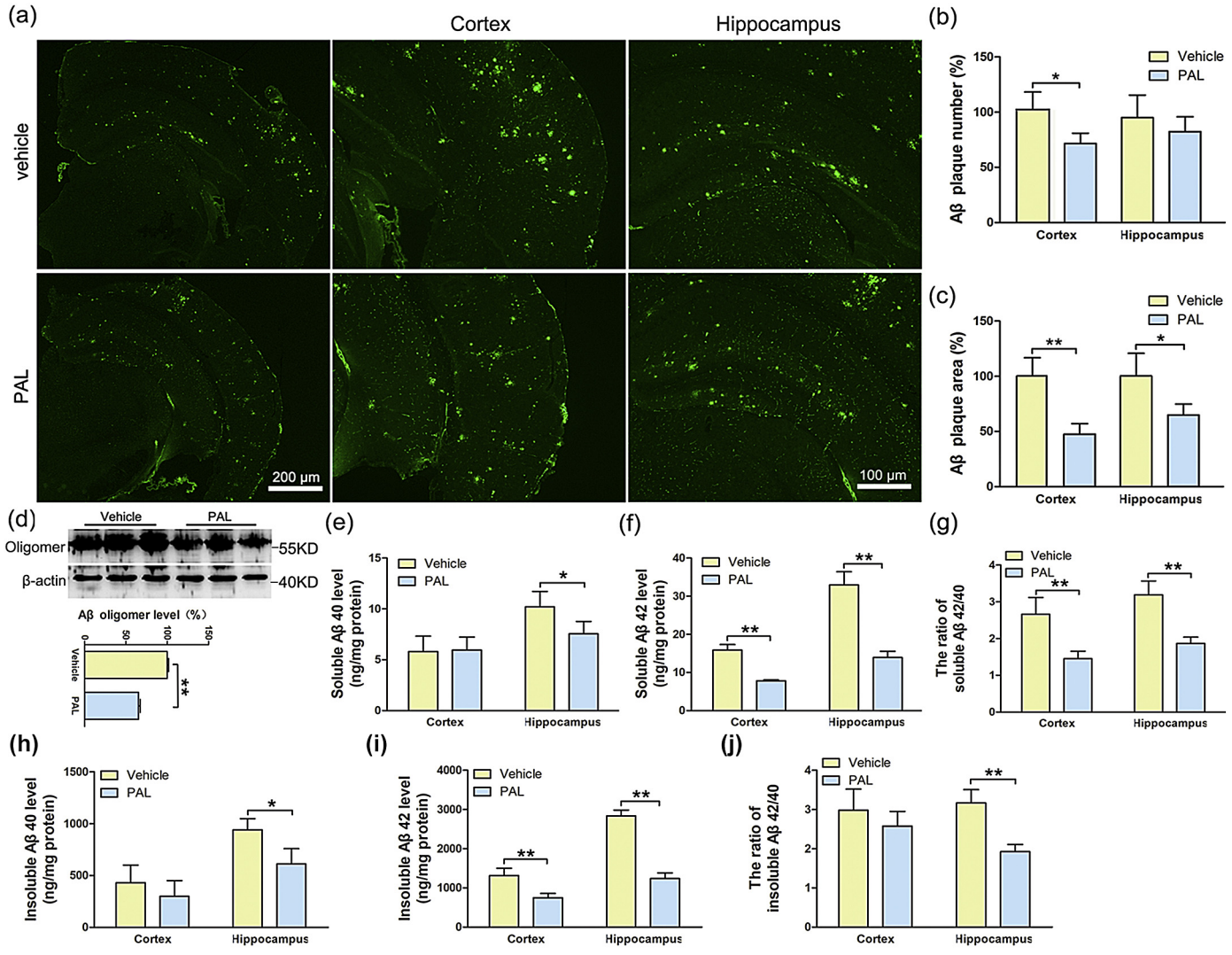

Fig. 2. PAL treatment reduces senile plaque burden in APP/PS1 mice. (a) Immunofluorescent labelling of Aβ showing the Aβ plaque in the cortex and hippocampus of APP/PS1 mice. Three sections/brain, $n = 6$. (b-c) Quantification of Aβ fluorescence revealed reduced number of Aβ plaque in the cortex and reduced areas of Aβ plaque in both the cortex and hippocampus of APP/PS1 mice after PAL treatment. (d) PAL treatment decreased Aβ oligomer protein levels. $n = 8$. (e-f) ELISA results showed a slight but significant reduction in Aβ40 in the hippocampus and a considerable reduction in Aβ42 in the cortex and hippocampus of APP/PS1 mice after PAL treatment. $n = 8$. (g) The ratios of soluble Aβ42/40 were decreased in both the cortex and hippocampus after PAL treatment. n = 8. (h-i) The insoluble Aβ40 was decreased in the hippocampus and the insoluble Aβ42 were reduced in both the cortex and hippocampus of APP/PS1 mice after PAL treatment. $n = 8$. (j) The ratio of insoluble Aβ42/40 was decreased in hippocampus after PAL treatment. n = 8. $^{*}p < .05$, $^{**}p < .01$ (Student's-*t*-test).

to ~48% (Fig. 3b), which was accompanied with a ~45% reduction of nuclear SREBP2 expression (Fig. 3c) in PAL treatment group compared to vehicle control group, indicating that PAL-induced reductions in SREBP2 expression are highly correlated with VDR activation in APP/PS1 mouse brains.

To further determine whether the decrease in Aβ generation and aggregation in APP/PS1 mice after PAL treatment is associated with APP-processing enzymes, we quantified the expression levels of ADAM10, BACE1 and PS1, which respectively correspond to α-, β- and γ-secretase. As shown in Fig. 3d, the expression levels of APP, ADAM10 and PS1 were not significantly different, but BACE1 expression levels were markedly decreased by ~46% after PAL treatment compared to those of the vehicle control; these findings suggest that BACE1 is the exclusive target enzyme of PAL that is responsible for the disturbance of Aβ generation. However, we did not find significant differences in the mRNA expression of BACE1 (Fig. 3f). Next, we evaluated the activities of α- and β-secretase based on their cleaved production of APP. The productions of sAPPα and C83 remained unchanged (Fig. 3e), whereas sAPPβ and C99 productions were respectively reduced to ~53% and 50% compared to that of the vehicle control (Fig. 3e). Furthermore, the

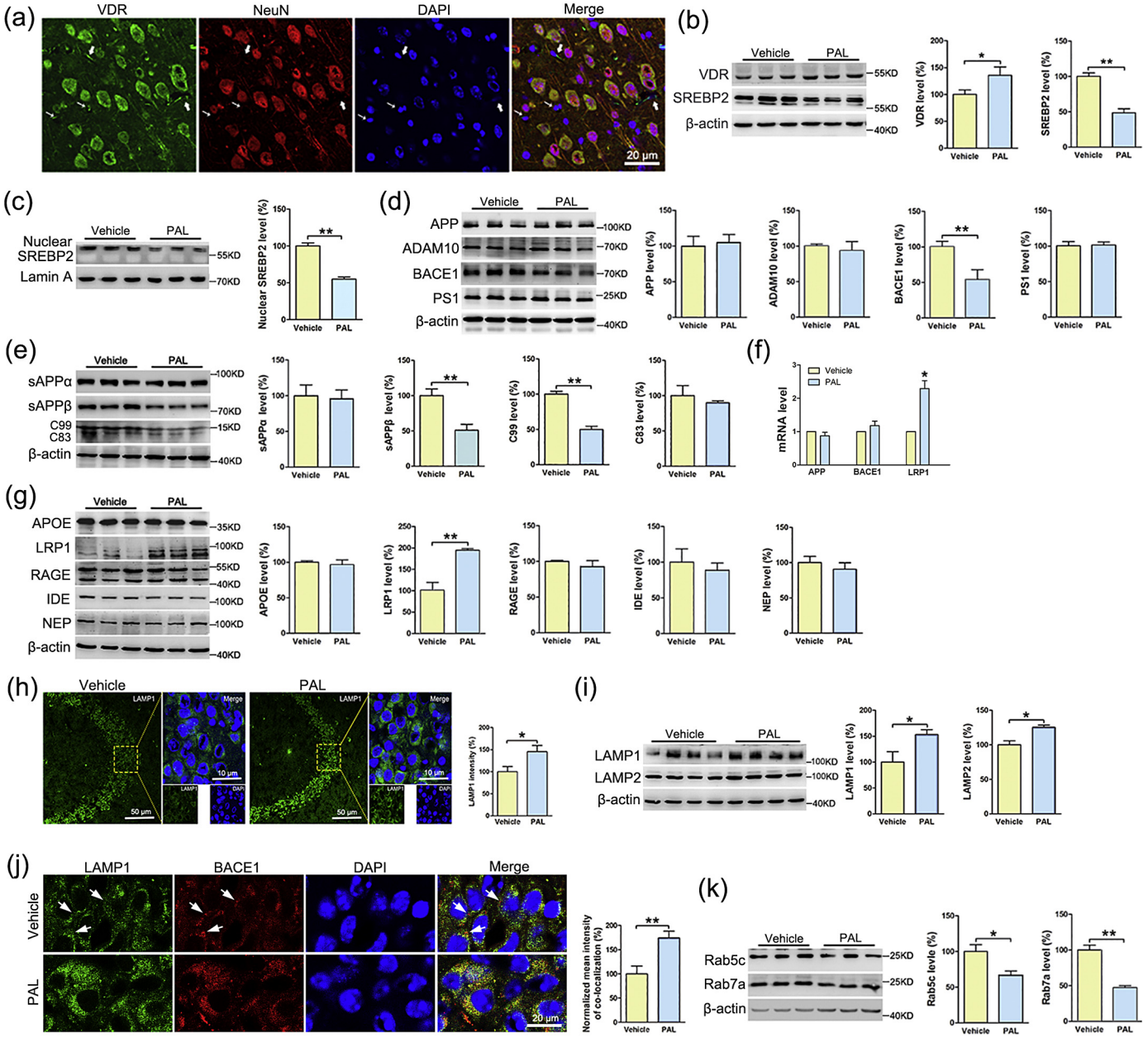

Fig. 3. PAL treatment decreases BACE1 expression in APP/PS1 mice. (a) Sections from APP/PS1 mouse brians were co-stained with VDR (green) and NeuN (red); the merged image from cortex shows the predominant localization of VDR in NeuN-positive neurons, and the large arrows and small arrows show the localization of VDR in the epithelium and glial cells, respectively. (b-c) Inhibition of total and nuclear SREBP2 were associated with VDR activation in the cortex of APP/PS1 mice. n = 8. (d) PAL treatment dramatically suppressed the expression of BACE1 but caused no significant differences in the protein levels of APP, ADAM10 or PS1 in APP/PS1 mouse brains. *n* = 8. (e) Immunoblotting showed that the protein levels of sAPPβ and C99 are decreased, but the protein levels of sAPPα and C83 are unchanged in APP/PS1 mouse brains after PAL treatment. n = 8. (f) APP and BACE1 mRNA expression levels were not significantly different in APP/PS1 mouse brains after PAL treatment. *n* = 6. (g) PAL treatment induced a marked upregulation of LRP1 without altering the expression of APOE, RAGE, IDE and NEP in APP/PS1 mouse brains. n = 8. (h) PAL treatment increased the immunointensity of LAMP1 in CA3 region. Three sections/brain, n = 6. (i) The lysosomal markers (LAMP1 and LAMP2) were increased in APP/PS1 mouse cortex after PAL treatment. n = 6. (j) Co-localizations of BACE1 and LAMP1 were increased in CA3 region after PAL treatment. The white arrows show BACE1 is not co-localized with LAMP1. Three sections/brain, *n* = 5. (k) The expression levels of rab5c (early endosomal marker) and rab7a (late endosomal marker) were significantly reduced in APP/PS1 mouse brains after PAL treatment. n = 8. $^{*}p < .05$, $^{**}p < .01$ (Student's-*t*-test).

γ-secretase activity was not significantly altered by PAL treatment (Supplementary Fig. 3). These data demonstrated that suppressing the protein levels and activity of BACE1 may be the main mechanism underlying PAL-mediated Aβ plaque reduction.

Aβ transport also plays a vital role in Aβ aggregation in the brain. We further examined the Aβ efflux protein LRP1, its ligand APOE, the Aβ influx protein RAGE, and the Aβ-degrading enzyme IDE and NEP. These proteins were unchanged, except for LRP1, its protein level and mRNA level were significantly increased after PAL treatment compared to vehicle control treatment (Fig. 3f, g). Interestingly, the lysosomal degradation of BACE1 can be induced by LRP1 [28]. In the present study, the lysosomal markers, LAMP1 and LAMP2 were respectively increased to ~153% and ~125% (Fig. 3i), and immunointensity of LAMP1 was also increased to ~145% in CA3 region after PAL treatment (Fig. 3h). Furthermore, immunostaining showed that PAL treatment causes a ~74% increase in the co-localization of BACE1 and LAMP1 in CA3 regions (Fig. 3j). The BACE1 targeting to lysosomes is impacted in Alzheimer's disease, which leads to accumulation of endosomes in neurons [24,49]. The expression levels of an early endosomal marker (Fig. 3k; rab5c; ~67% of vehicle control) and a late endosomal marker (Fig. 3 k; rab7a; ~47% of vehicle control) were decreased in PAL treated mice. These data suggest that PAL treatment may promote BACE1 lysosomal targeting and stimulates Aβ elimination via upregulating LRP1 in APP/PS1 mouse brains.

3.4. PAL downregulates BACE1 expression via promoting BACE1 lysosomal degradation in N2a-sw cells

Next, we used N2a-sw cells to further explore the mechanism of PAL-induced BACE1 downregulation. As expected, PAL treatment caused no cytotoxicity to these cells (Fig. 4a). PAL slightly but significantly reduced the amount of Aβ42 (Fig. 4b; ~88% of vehicle control) that was secreted into the culture medium. VDR expression was robustly increased to ~220% after PAL treatment (Fig. 4c). Meanwhile, PAL treatment dramatically downregulated the expression of BACE1 in a dose-dependent manner (Fig. 4d; ~69% - 32% of vehicle control) without altering the expression of APP, ADAM10 or PS1 (Fig. 4d). The cycloheximide chase experiments also revealed that PAL treatment reduces the halflife of BACE1 (vehicle = 14.8 ± 1.1 vs PAL = 11.1 ± 0.9) compared to vehicle control in N2a-sw cells (Supplementary Fig. 4). Furthermore, SREBP2 was reduced (Fig. 4e; ~75% - 52% of vehicle control) in parallel with LRP1 upregulation (Fig. 4e, f; ~169% of vehicle control) following PAL treatment, suggesting that PAL upregulates LRP1 expression via inhibiting SREBP2 in neurons. However, we did not find significant changes in BACE1 mRNA expression (Fig. 4f), indicating that PAL post-transcriptionally regulated BACE1 in N2a-sw cells.

Since LRP1 interacts with BACE1 to promote BACE1 targeting to late endosomes for lysosomal degradation [28], we speculated that PAL treatment downregulates BACE1 via upregulation of LRP1. As shown

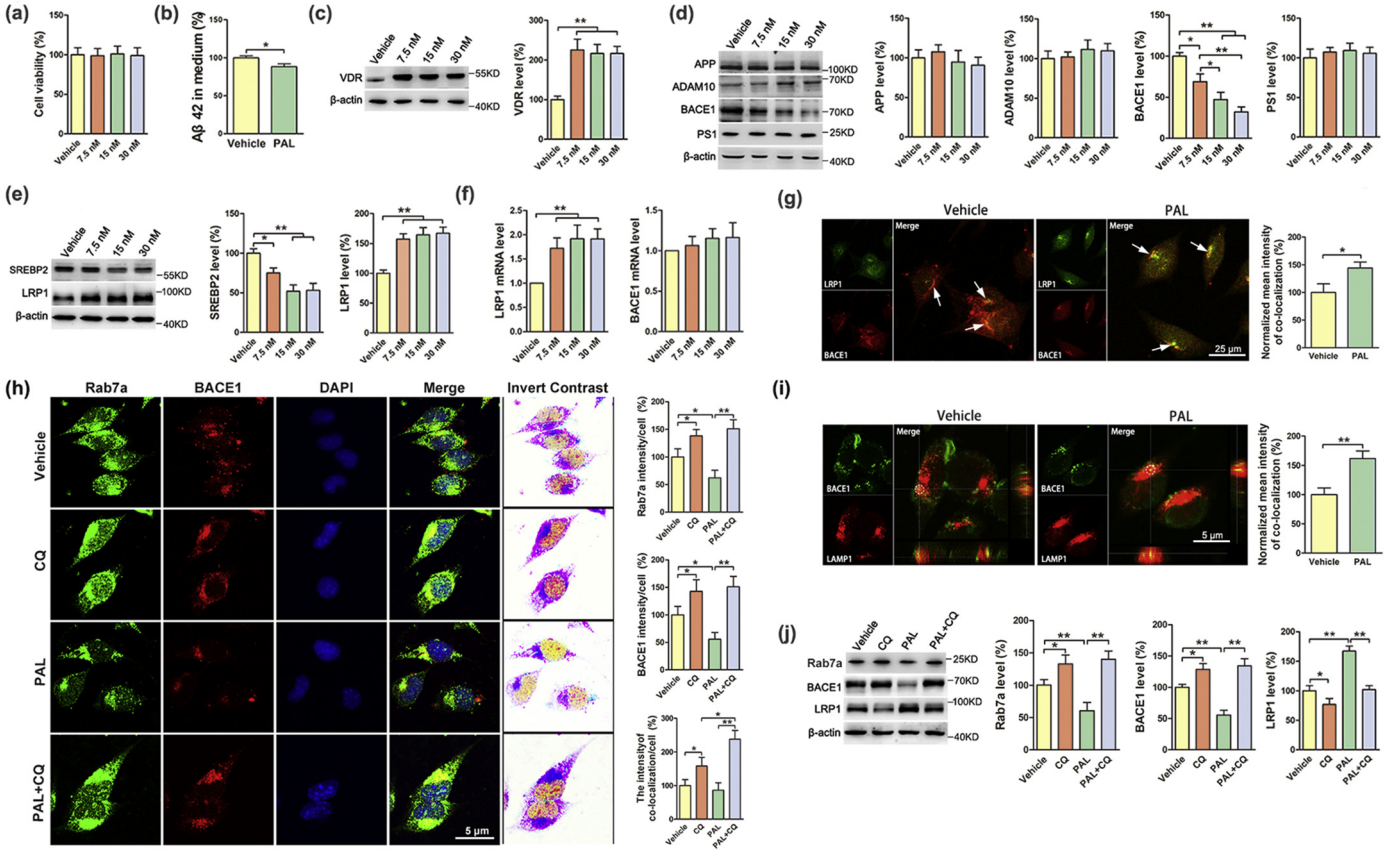

Fig. 4. PAL downregulates BACE1 expression via promoting BACE1 lysosomal degradation in N2a-sw cells. (a) MTT assays showed that 0–30 nM PAL treatment caused no cytoxicity in N2a-sw cells. *p < .05 (Student's-*t*-test). (b) According to sandwich ELISA results, the concentration of Aβ42 in the medium was significantly decreased after 15 nM PAL treatment for 24 h. *p < .05 (Student's-*t*-test). (c-e) Immunoblotting results showing the protein levels of VDR, APP, ADAM10, BACE1, PS1, SREBP2 and LRP1 in N2a-sw cells after 0–30 nM PAL treatment for 24 h. *p < .05, **p < .01 (one-way ANOVA). (f) Real-time PCR results showing the mRNA expression of LRP1 and BACE1. **p < .01 (one-way ANOVA). (g) The co-localization of BACE1 (red) and LRP1 (green) was increased in N2a-sw cells after PAL treatment. The arrows indicate the co-localization of BACE1 with LRP1. *p < .05 (Student's-*t*-test). (h) The co-localizations of BACE1 (red) with Rab7a (green) were analysed in PAL (15 nM) and/or CQ (20 μM) treated cells. At least thirty cells were quantified per group. *p < .05, **p < .01 (one-way ANOVA). (i) The co-localization of BACE1 (green) with LAMP1 (red) was increased in 15 nM PAL-treated cells compared to vehicle control. White circles showing the BACE1 co-localized with Rab7a and LAMP1. At least thirty cells were quantified per group. **p < .01 (Student's-*t*-test). (j) Co-incubation with PAL (15 nM) and chloroquine (CQ; 20 μM) for 24 h in N2a-sw cells abrogated the altered BACE1 and LRP1 expression levels caused by PAL treatment only. *p < .05, **p < .01 (one-way ANOVA).

in Fig. 4g, PAL treatment leaded to a ~45% increase in the co-localized intensity of LRP1 and BACE1 compared to vehicle control. Moreover, PAL-induced BACE1 reduction was abrogated by LRP1 knockdown (Supplementary Fig. 5). Immunostaing revealed that although the co-localizations of Rab7a and BACE1 in vehicle control and PAL-treated cells were similar, PAL treatment combined with a lysosomotropic reagent chloroquine (CQ) clearly increased the BACE1 located in late endosomes compared to PAL-treated cells (Fig. 4h). Meanwhile, PAL treatment combined with CQ also significantly elevated the co-localization of BACE1 with Rab7a compared to CQ treatment (Fig. 4h). These data suggested that PAL treatment promotes BACE1 targeting to late endosomes. In addition, PAL treatment also caused a ~61% increase in the co-localization of BACE1 and LAMP1 compared to vehicle control (Fig. 4i). We then used CQ to further verify the PAL-induced BACE1 lysosomal degradation. As shown in Fig. 4j, the PAL-induced BACE1 reduction was almost completely rescued after CQ treatment. These data demonstrated that PAL treatment promotes BACE1 targeting to late endosomes for lysosomal degradation via upregulating LRP1 expression. Interestingly, we found a significant reduction in LRP1 expression after CQ treatment only or CQ treatment combined with PAL. These results indicated that the disruption of lysosomal function may have a role in regulating LRP1, and they confirm that LRP1 does not undergo lysosomal degradation as reported before [28,50].

3.5. PAL treatment diminishes 8-OHdG generation in neuronal mitochondria via improved BER

Due to our finding that Aβ aggregation was decreased by accelerating LRP1-dependent clearance and BACE1 lysosomal degradation, we next sought to determine the neuroprotective mechanism of PAL. mtDNA mutations are highly associated with ageing and neurodegenerative diseases. Error-avoiding mechanisms protect mitochondria from oxidative-induced mtDNA mutations and maintain mitochondrial functions. As 8-OHdG is a main contributor to oxidative damage, we analysed the expression of OGG1, MTH1, and MUTYH, which prevent 8-OHdG-induced mtDNA mutations. As shown in Fig. 5a, OGG1 and MTH1 expression levels were dramatically increased by ~42% and ~119%, respectively, while MUTYH expression was largely downregulated (~63% of vehicle control) in PAL-treated mice compared to vehicle control-treated mice. We then visualized the expression of 8-OHdG in mitochondria using immunofluorescence, images showed that the 8-OHdG was highly co-localized with mitochondrial markers COX4 and P450 (Supplementary Fig. 6). The fluorescence intensity of 8-OHdG was strongly reduced to ~53% after PAL treatment (Fig. 5b). To identify whether 8-OHdG was reduced predominantly in neuronal mitochondria, we co-stained 8-OHdG and NeuN. Images revealed that 8-OHdG was mostly co-localized with NeuN-positive cells, and the relative 8-OHdG fluorescent index confirmed the reduction in 8-OHdG in neuronal mitochondria after PAL treatment (Fig. 5c). These data demonstrated that PAL strongly diminishes 8-OHdG generation in neuronal mitochondria via upregulating OGG1 and MTH1.

3.6. Inhibition of caspase- and calpain-dependent neuronal loss after PAL treatment

Neuronal loss mediated by caspase-dependent apoptosis is a key feature of Alzheimer's disease progression. As mtDNA damage in mitochondria was rescued by PAL treatment in neurons, we hypothesized that PAL may play a role in regulating mitochondria-induced apoptosis via changing the expression of Bcl-2 family proteins. Interestingly, although activated caspase-3 (Fig. 6a; ~70% of vehicle control) was downregulated after PAL treatment, the expression levels of Bax and Bcl-2 were not altered (Fig. 6a), suggesting that the caspase-dependent apoptosis attenuated by PAL is independent of Bcl family proteins and involved other mechanisms. Notably, PAL effectively downregulates MUTYH (Fig. 5a), and 8-oxoG induces MUTYH-initiated cell death in a calpain-dependent manner [40,42]; herein, we quantified calpain-1 expression and its enzymic activity using immunoblotting. As shown in Fig. 6b, calpain-1 was significantly reduced to ~70% after PAL treatment. To assess the enzymic activity of calpain-1, we analysed the cleaved product (145 KD) of α-spectrin, a specific hydrolytic product of calpain-1. As shown in Fig. 6b, the cleaved product of α-spectrin was decreased to ~54% after PAL treatment, indicating that calpain-1 activity is inhibited by PAL. Ectopic calpain-1 activation induces lysosomal rupture and subsequently leads to cell death [40,42]. The lysosomal content were significantly increased after PAL treatment in APP/PS1 mouse brains (Fig. 3h, i), indicating that PAL may inhibit lysosomal rupture via targeting calpain-1. HSP70 is localized at the lysosomal membranes which is indispensable for stabilizing the lysosomal membranes. Activated calpain-1 induces lysosomal rupture via cleavage of full-length HSP70 [51]. Interestingly, the full-length HSP70 was significantly increased after PAL treatment (Fig. 6b). Moreover, cathepsin D, a hydrolytic cathepsin enzyme typically sequestered within lysosomes, were largely leaked from lysosomes in APP/PS1 mouse brains, however, PAL treatment significantly reversed this phenomenon (Fig. 6c). Our data suggested that PAL treatment inhibits calpain-1-meidated lysosomal rupture in APP/PS1 mouse brains. Consequently, the expression levels of NeuN (Fig. 6d; ~144% of vehicle control) and synaptic markers (Fig. 6d; SYP, ~131% of vehicle control and PSD95, ~136% of vehicle control) were significantly increased by PAL treatment compared to vehicle control treatment. Immunohistochemical staining also revealed that PAL treatment increases the NeuN positive cells in cortex (Fig. 6e; ~135% of vehicle control) and SYP intensities in cortex (Fig. 6f; ~150% of vehicle control) and CA1 region (Fig. 6f; ~155% of vehicle control) compared to vehicle control, further confirming that PAL inhibits neuronal death and synaptic loss.

3.7. PAL treatment reduces Aβ42 oligomer-induced cell death in N2a cells

In order to elucidate whether PAL has a direct role in the regulation of mitochondrial 8-OHdG-induced cell death in the pathology of Alzheimer's disease, we further evaluated the effects of PAL on Aβ42 oligomer-treated N2a cells. Our results revealed that the Aβ42 oligomer treatment clearly reduced the expressions of OGG1 and MTH1 in N2a cells (Fig. 7a). Meanwhile, the expressions of MUTYH and calpain-1 were significantly increased in Aβ42 oligomer-treated cells compared to vehicle control (Fig. 7a, b). However, PAL treatment significantly rescued these effects mediated by Aβ42 oligomer (Fig. 7a, b). As expected, PAL treatment effectively reduced the Aβ42 oligomer-induced mitochondrial 8-OHdG generation in N2a cells (Fig. 7c, d). These data suggested that PAL could directly regulate mitochondrial 8-OHdG generation via targeting BER. In addition, consistent with the effects of calpain-1 inhibition, PAL treatment significantly increased the cell viability and decreased the death rate in Aβ42 oligomer-treated cells (Fig. 7e, f), indicating that PAL could reduce Aβ toxicity-induced cell death.

3.8. PAL treatment alleviates inflammatory stress

Ectopic inflammatory responses are crucial for the progression of Alzheimer's disease, and excessive amounts of inflammatory factors secreted by active microglia and astrocytes exacerbate Aβ-induced cell damage. As shown in Fig. 8a, the IL-1β (~64% of vehicle control) and TNFα (~48% of vehicle control) were significantly reduced after PAL treatment. Immunostaining also revealed that PAL treatment reduced the numbers of active microglia and astrocytes around Aβ plaques (Fig. 8b). These results indicated that the ectopic inflammatory stress induced by Aβ aggregation was inhibited by PAL treatment.

4. Discussion

Clinical investigations have shown that vitamin D supplementation effectively ameliorates the process of Alzheimer's disease by improving

cognitive ability [4,5,52]. However, the mechanism through which vitamin D inhibits Alzheimer's disease remains unknown. It is well recognized that altering Aβ production and/or clearance is an important strategy for Alzheimer's disease therapy. In this study, we found that long-term treatment with PAL clearly attenuated Aβ deposition via downregulating Aβ42 production; PAL also suppressed neuronal death and, most importantly, rescued cognitive impairment in APP/PS1 mice.

It has been reported that vitamin D insufficiency increases the risk of developing Alzheimer's disease [53,54] and that supplementation with vitamin D or VDR overexpression suppresses the promoter activity of APP in neuroblastoma cells [54]. However, in this study, APP protein levels were not altered after PAL treatment in either APP/PS1 mice or N2a-sw cells, despite increased VDR expression levels. In fact, VDR was recently identified as a transcriptional regulator of genes involved in APP processing. VDR silencing significantly increased the mRNA expression levels of ADAM10, BACE1 and PS1, while vitamin D repressed the expression of these mRNAs and subsequently reduced the production of Aβ42 in primary neurons [55]. Interestingly, the soluble Aβ42 was clearly reduced in both the cortex and hippocampus without influencing the concentration of soluble Aβ40 in cortex after PAL treatment. The APP/PS1 mice are characterized by higher production of Aβ42 than Aβ40, the inequality of Aβ40 and Aβ42 production may lead to different drug tolerance between Aβ40 and Aβ42. Indeed, the different alternations between Aβ42 and Aβ40 after drugs treatment were observed in many studies [56,57]. The expressions of the major secretases involved in APP processing were examined. Among these proteins, only BACE1 protein level was sharply downregulated in APP/PS1 mice after PAL treatment. Interestingly, the mRNA expression of BACE1 was not altered, suggesting that PAL post-transcriptionally regulate BACE1 expression.

BACE1 is abundantly localized in neuronal axons and dendrites [58]; there, APP is hydrolysed to Aβ and subsequently released into the extracellular region [59]. Mature BACE1 can be endocytosed to early

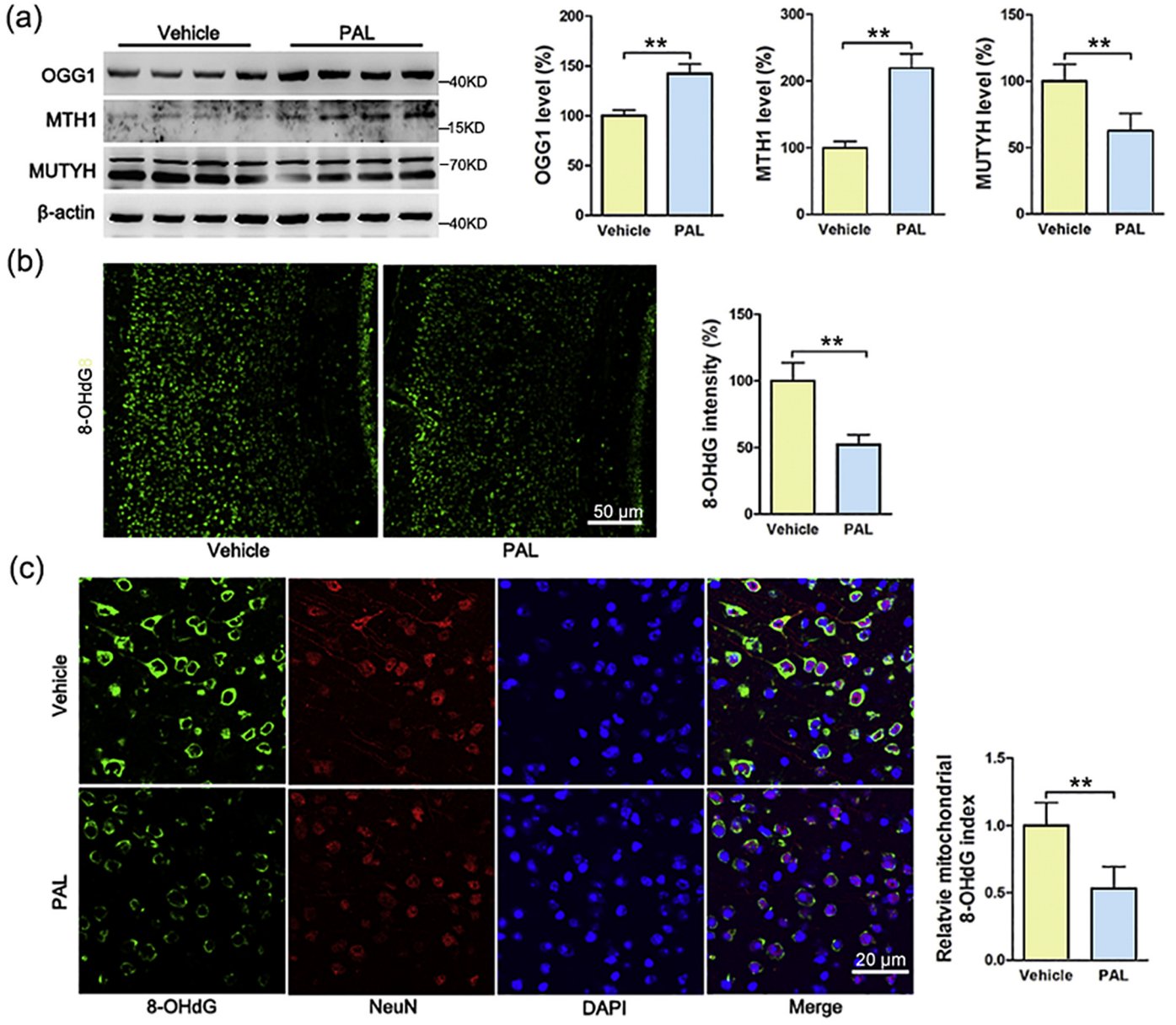

Fig. 5. PAL treatment diminishes 8-OHdG generation in neuronal mitochondria via improved BER. (a) PAL treatment markedly increased the expression of OGG1 and MTH1 but suppressed the expression of MUTYH in APP/PS1 mouse brains. n = 8. (b) Mitochondrial 8-OHdG generation was inhibited in APP/PS1 mouse brains after PAL treatment. Three sections/brain, n = 6. (c) PAL treatment dramatically suppressed mitochondrial 8-OHdG generation in NeuN-positive neurons from APP/PS1 mouse brains. Three sections/brain, n = 6. **p < .01 (Student's-*t*-test).

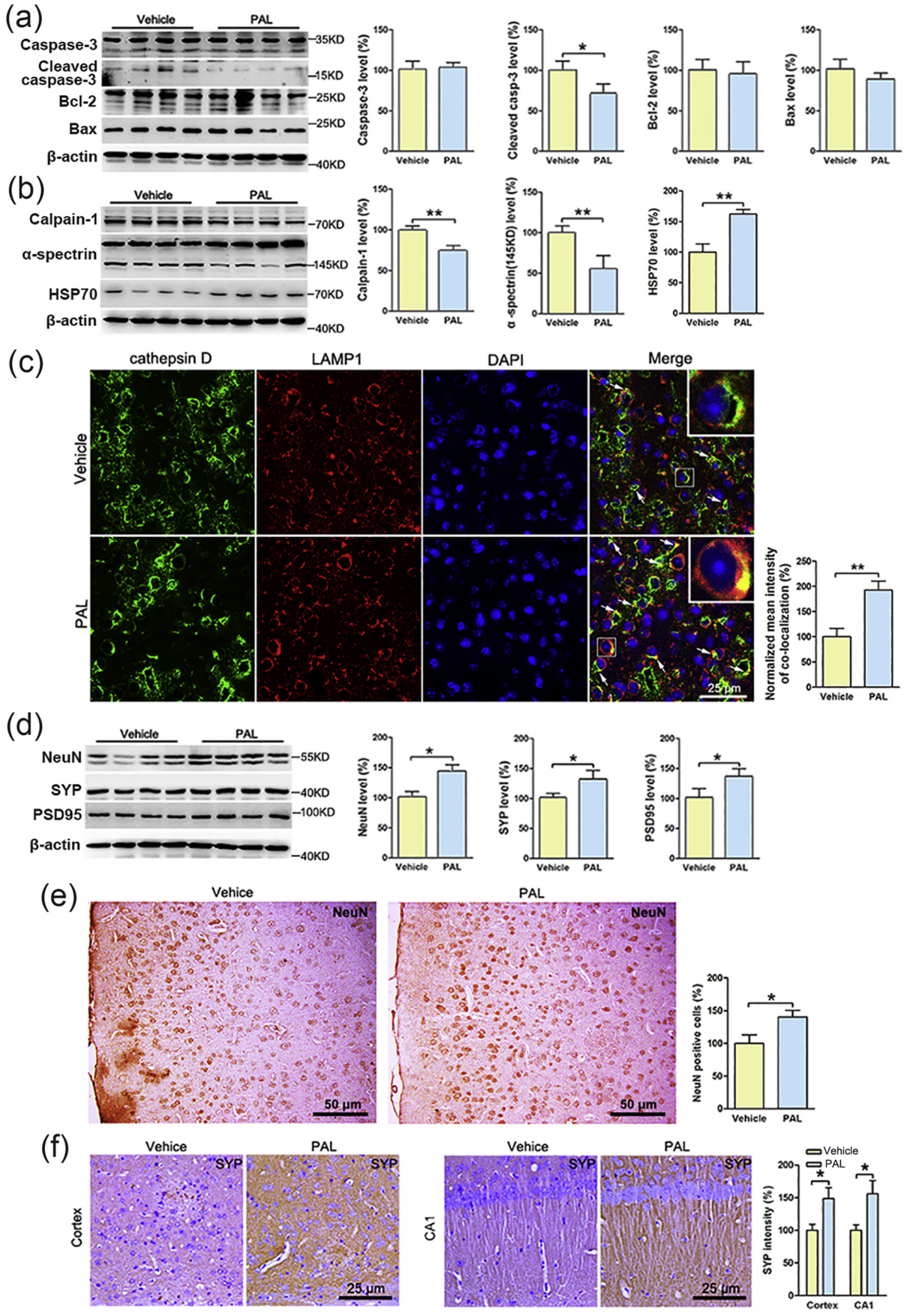

Fig. 6. Inhibition of caspase- and calpain-dependent neuronal loss after PAL treatment. (a) Caspase-3 inhibition was independent of Bcl family proteins (Bcl-2 and Bax) in APP/PS1 mouse brains after PAL treatment. n = 8. (b) PAL treatment suppressed the expressions of calpain-1 and α-spectrin (145 KD), whereas increased the expression of full-length HSP70. n = 8. (c) PAL treatment increased the co-localization of cathepsin D (green) with LAMP1 (red). Three sections/brain, n = 5. (d) NeuN, SYP and PSD95 upregulation were induced by PAL treatment, n = 8. (e-f) NeuN positive cells in cortex and SYP intensities in cortex and CA1 region were increased after PAL treatment. Three sections/brain, n = 5. *p < .05, **p < .01 (Student's-*t*-test).

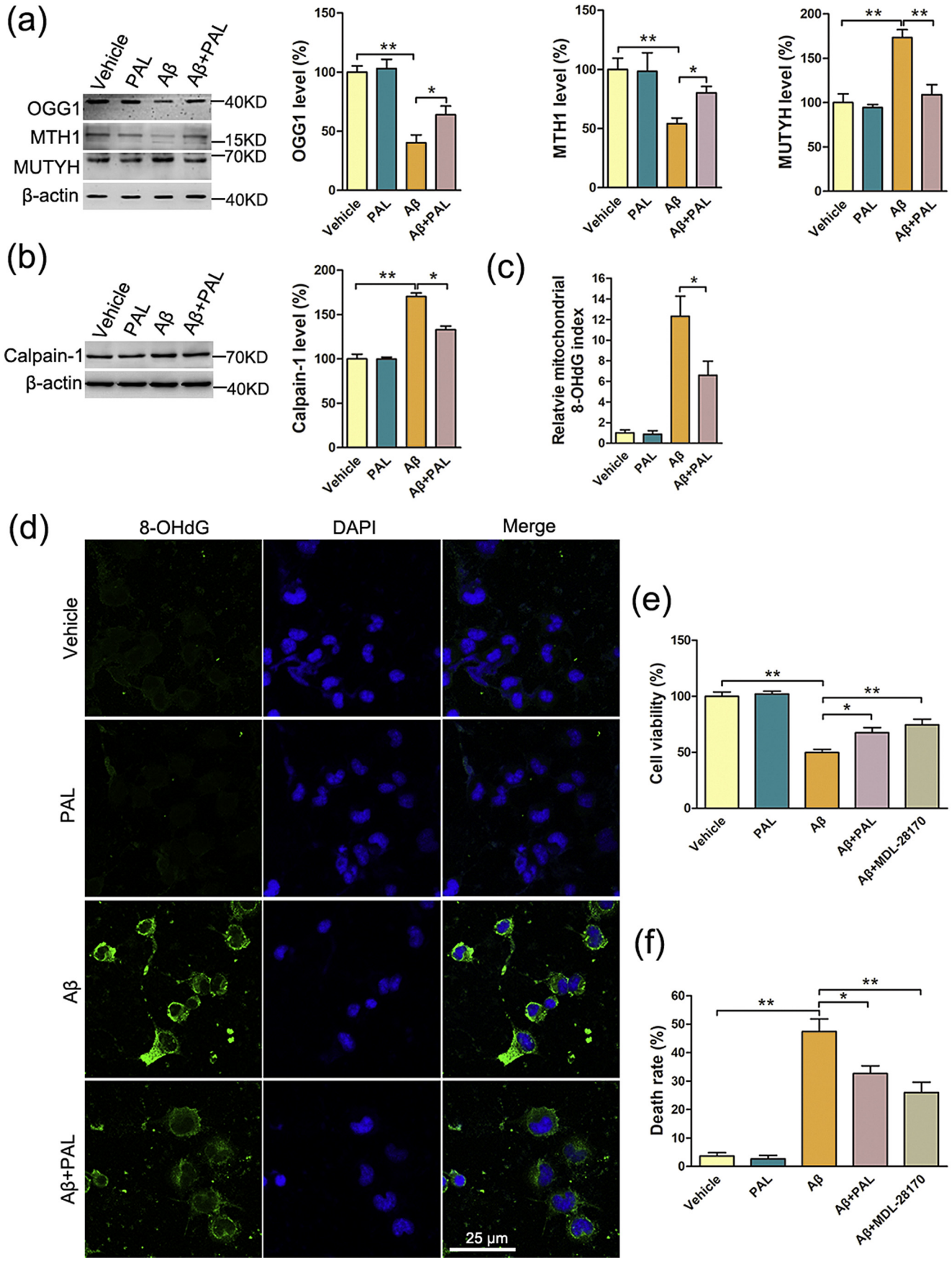

Fig. 7. PAL treatment reduces Aβ42 oligomer-induced cell death in N2a cells. (a-b) PAL treatment (15 nM) rescued the Aβ42 oligomer (2 μM)-induced OGG1 and MTH1 downregulations as well as MUTYH and calpain-1 upregulations. (c-d) PAL treatment reduced the Aβ42 oligomer-induced mitochondrial 8-OHdG generation in N2a cells. (e) PAL treatment increased the cell viability in Aβ42 oligomer-treated N2a cells. (f) PAL treatment decreased Aβ42 oligomer-induced cell death in N2a cells. $n = 3$. *p < .05, **p < .01 (Student's-*t*-test).

endosomes and then transferred to late endosomes for lysosomal degradation [20,28]. Elevated BACE1 expression was found in Alzheimer's disease brains because of the impaired lysosomal degradation of BACE1 [24]. Here, we demonstrated that PAL treatment promotes BACE1 targeting to late endosomes for lysosomal degradation in vivo and in vitro. BACE1 expression is predominantly modulated by post-translational regulations. BACE1 can be modified with bisecting *N*-acetylglucosamine (GlcNAc), which stabilizes BACE1 to avoid lysosomal degradation in Alzheimer's disease brains [60]. BACE1 can also be phosphorylated at Ser498 in its cytoplasmic domain, which promotes the interaction of BACE1 and GGA1, thereby modulating BACE1 intracellular trafficking [61]. Despite the direct modifications of BACE1, proteins can also directly interact with BACE1 to promote lysosomal degradation of BACE1 [24,28]. Snapin, as a dynein motor adaptor for late endosomes, directly interacts with BACE1 to mediate BACE1 retrograde transport [24]. LRP1 is highly localized to neurons and reported to be a substrate of BACE1 [62,63] and that LRP1 is also recognized as an endocytic receptor [64]. Recent study revealed that LRP1 interacts with BACE1 to decrease the protein stability and membrane association of BACE1, which subsequently facilitates the transition of BACE1 from early endosomes to late endosomes for lysosomal degradation [28]. The expression of LRP1 was considerably upregulated after PAL treatment, thus, we concluded that LRP1-mediated BACE1 lysosomal degradation is the main cause of PAL-mediated SP reductions in APP/PS1 mice.

Impaired Aβ efflux in the brain accelerates the progression of Alzheimer's disease. Endothelial LRP1 interacts with Aβ and mediates Aβ transcytosis through the blood-brain barrier; thus, LRP1 is widely recognized as the most important transporter for Aβ efflux [26,27]. Specific deletion of LRP1 in forebrain neurons exacerbates Aβ aggregation in cortex without affecting Aβ production and Aβ degradation enzymes; these findings highlight the great importance of LRP1 in the neuronal clearance of Aβ [64]. However, LRP1 regulation remains poorly understood. SREBP2 is recognized as the only transcriptional repressor of LRP1, and increased nuclear SREBP2 expression leads to LRP1 downregulation, which impairs Aβ clearance in Alzheimer's disease patients [65]. Interestingly, a recent study demonstrated that 25-hydroxyvitamin D (25OHD), one of the hydroxylated vitamin D metabolites, decreases SREBP2 level independent of the VDR [66]. However, this study also provided the evidence that the mechanism of $1,25(OH)_2$ D-induced SREBP2 downregulation is different from 25OHD-induced SREBP2

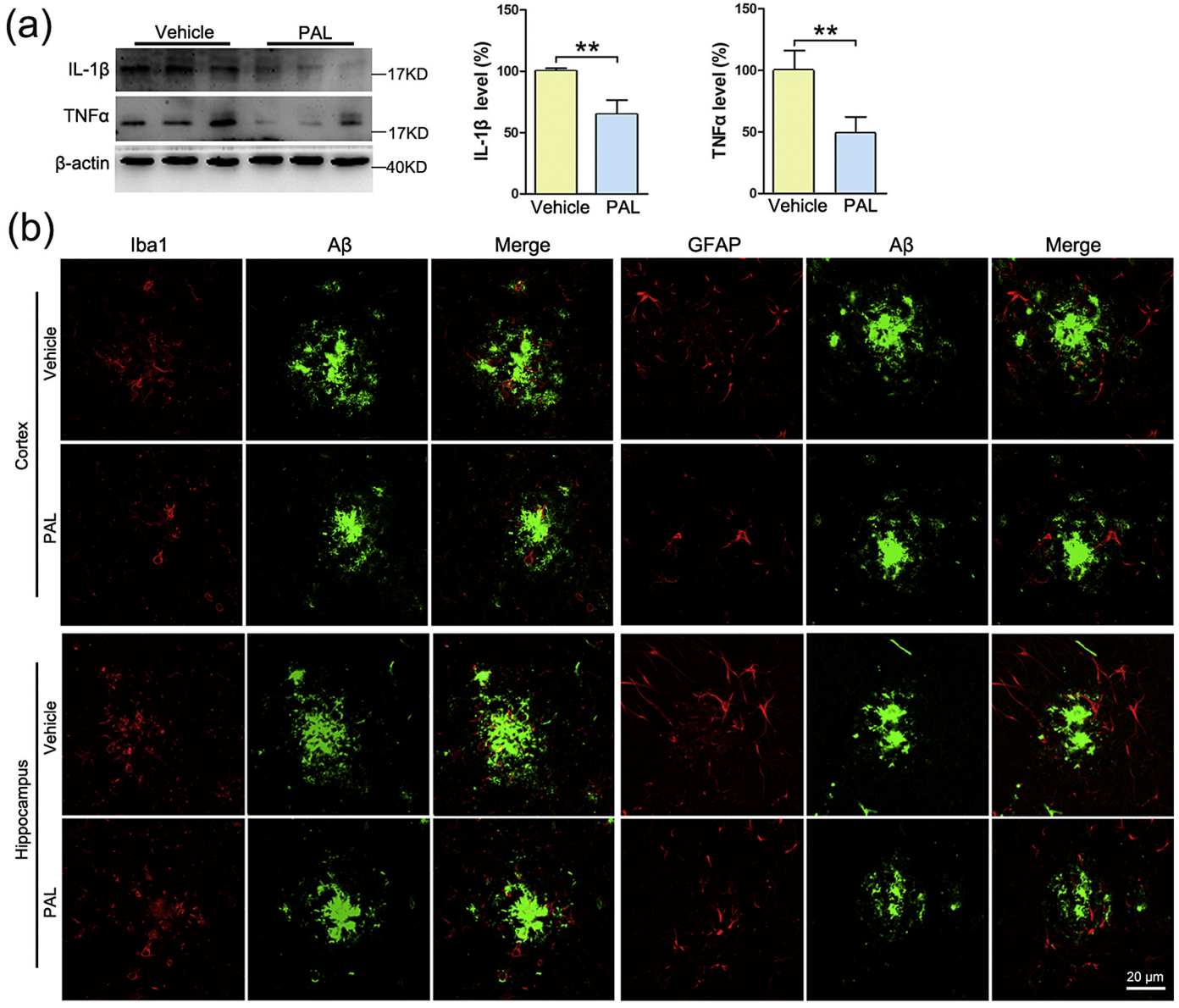

Fig. 8. PAL treatment alleviates inflammatory stress. (a) IL-1β and TNFα were decreased after PAL treatment. n = 8. (b) PAL treatment alleviated the activations of microglia and astrocytes around Aβ plaque. Three sections/brain, n = 5. **p < .01 (Student's-*t*-test).

downregulation [66]. Since $1,25(OH)_2$ D is the most potent endogenous VDR ligand, this study also indicated that VDR may be a repressor of SREBP2. Consistent with this study, the increased SREBP2 expression was found in the mice with decreased VDR transcriptional activity [67]. Moreover, the VDR agonist doxercalciferol also decreased the SREBP2 expression in dietary fat-induced renal disease [31]. SREBP2 expression was decreased in PAL-treated mice, thus we suggest that PAL upregulates LRP1 expression in vivo and in vitro, possibly through targeting SREBP2. In line with our observation, Guo et al. [68] demonstrated that LRP1 was increased in mouse brain microvascular endothelial cells after vitamin D exposure. On the other hand, Durk et al. [7] reported that vitamin D induced P-glycoprotein (P-gp) expression to mediate Aβ efflux in Tg2576 mice without affecting LRP1 or RAGE expression. The reason for these conflicting observations is unclear but may be related to the differences in the animal models used in these studies. APOE is a competitive ligand for Aβ binding to LRP1 in the interstitial fluid and subsequently influences soluble Aβ metabolism [69]. APOE levels were not changed in our experiment, suggesting that the increased LRP1 expression is conducive to forming the LRP1-Aβ complex, which is a critical step for Aβ clearance. Thus, our results strongly suggest that PAL eliminates Aβ in the brains of APP/PS1 mice through upregulating LRP1.

Neuronal degeneration is an event down-stream of Aβ toxicity. As expected, we also found that PAL is a strong neuroprotective agent that protects neurons from neuronal degeneration in APP/PS1 mice and in response to Aβ. Calpains are a family of Ca^{2+}-activated cysteine proteases closely linked with Alzheimer's disease. Inhibiting calpain-1 effectively suppresses neuronal death mediated by Ca^{2+} loading or oxidative stress [70,71]. Moreover, calpain-1 activity is increased throughout the progression of Alzheimer's disease [72] and inhibiting calpain-1 relieves Alzheimer's disease pathology in an animal model of Alzheimer's disease [73]; these findings indicate that the suppression of calpain-1 is an attractive strategy for Alzheimer's disease treatment. Notably, OGG1 and/or MTH1 deficiency contributes to 8-oxoG accumulation in mitochondria and subsequently leads to calpain-1-induced lysosomal rupture and neuronal loss under oxidative stress conditions [42]. Our findings in the present study show that OGG1 and MTH1 expression levels were dramatically increased, and MUTYH was downregulated in PAL-treated mice compared to vehicle control-treated mice; these effects reduced mitochondrial 8-OHdG in neurons. Lysosomal rupture was eventually reduced in PAL-treated mice, consistent with previous findings that 8-OHdG generation in mitochondria induces mitochondrial dysfunction and subsequently causes Ca^{2+} release from mitochondria to induce calpain-1-meidated lysosomal rupture [40,42]. Active caspase-3 levels were significantly decreased in PAL-treated mice compared to vehicle control-treated mice. However, we found no differences in the expression levels of Bcl family proteins, suggesting that PAL inhibits neuronal apoptosis via suppressing caspase-3 activation, independent of changes in Bcl family proteins. It has been demonstrated that calpain-1 regulates apoptosis via activating caspase-3 [71], but mitochondrial 8-oxoG-induced cell death is independent of caspase-3 activation [40,42]. Calpain-1 but not caspase-3 activity is increased throughout Alzheimer's disease progression [72], indicating that calpain-1 regulates neuronal death in Alzheimer's disease independent of caspase-3. The expression levels of post-mitotic neuronal and synaptic markers were significantly higher in the PAL treatment group than in the vehicle control treatment group, demonstrating that neuronal loss was inhibited after PAL treatment. Therefore, we infer that PAL treatment suppresses neuronal death via inhibiting caspase-3 activation as well as calpain-1 activation by inhibiting the generation of 8-OHdG in neuronal mitochondria. Of note, PAL treatment effectively reduces lysosomal rupture in APP/PS1 mouse brains. Considering that BACE1 is predominantly degraded in lysosomes [24,28], inhibition of lysosomal rupture can be another mechanism in PAL-mediated BACE1 reduction.

In summary, our study found that PAL treatment markedly improves cognitive ability in APP/PS1 mice. Mechanistic studies show that PAL treatment dramatically upregulates LRP1 expression via inhibiting SREBP2; increased LRP1 expression levels in neurons promote the LRP1-mediated BACE1 lysosomal degradation, resulting in reduced Aβ production. Furthermore, PAL treatment effectively protected mtDNA from 8-OHdG-mediated spontaneous mutations via upregulating OGG1 and MTH1 expression, which abrogates calpain-1-mediated neuronal death.

Acknowledgements

The funders had no role in study design, data collection, data analysis, interpretation and writing of the report.

Declaration of interests

The authors declare that they have no competing interests.

Funding sources

This study was financially supported by the Natural Science Foundation of China (U1608282).

Author contributions

Y.G.F., performed most of the experiments and analysed the data; T. G and X.R.H., contributed to experiments; J.L.L., Y.T.C., and H.X., generated and validated the mouse model; Y.C.L., and X.S.H., contributed to discussion; Z.Y.W., reviewed and edited manuscript; C. G., designed and wrote manuscript. All authors have read and approved the final manuscript.

Appendix A. Supplementary data

Supplementary data to this article can be found online at https://doi.org/10.1016/j.ebiom.2019.07.014.

References

[1] Bouillon R. Genetic and environmental determinants of vitamin D status. Lancet 2010;376:148–9.
[2] Jayedi A, Rashidy-Pour A, Shab-Bidar S. Vitamin D status and risk of dementia and Alzheimer's disease: a meta-analysis of dose-response. Nutr Neurosci 2018:1–10.
[3] Aspell N, Lawlor B, O'Sullivan M. Is there a role for vitamin D in supporting cognitive function as we age? Proc Nutr Soc 2017:1–11.
[4] Annweiler C, Rolland Y, Schott AM, et al. Higher vitamin D dietary intake is associated with lower risk of alzheimer's disease: a 7-year follow-up. J Gerontol A Biol Sci Med Sci 2012;67:1205–11.
[5] Annweiler C, Fantino B, Gautier J, Beaudenon M, Thiery S, Beauchet O. Cognitive effects of vitamin D supplementation in older outpatients visiting a memory clinic: a pre-post study. J Am Geriatr Soc 2012;60:793–5.
[6] Miller BJ, Whisner CM, Johnston CS. Vitamin D supplementation appears to increase plasma Abeta40 in vitamin D insufficient older adults: a pilot randomized controlled trial. J Alzheimers Dis 2016;52:843–7.
[7] Durk MR, Han K. E.C. Chow, et al. 1alpha,25-Dihydroxyvitamin D3 reduces cerebral amyloid-beta accumulation and improves cognition in mouse models of Alzheimer's disease. J Neurosci 2014;34:7091–101.
[8] Kim MS, Lee S, Jung N, et al. The vitamin D analogue paricalcitol attenuates hepatic ischemia/reperfusion injury through down-regulation of toll-like receptor 4 signaling in rats. Arch Med Sci 2017;13:459–69.
[9] Uyanikgil Y, Solmaz V, Cavusoglu T, et al. Inhibitor effect of paricalcitol in rat model of pentylenetetrazol-induced seizures. Naunyn Schmiedeberg's Arch Pharmacol 2016;389:1117–22.
[10] Ito S, Ohtsuki S, Nezu Y, Koitabashi Y, Murata S, Terasaki T. 1alpha,25-Dihydroxyvitamin D3 enhances cerebral clearance of human amyloid-beta peptide (1–40) from mouse brain across the blood-brain barrier. Fluids Barriers CNS 2011;8:20.
[11] Cheng J, Rui Y, Qin L, et al. Vitamin D combined with resveratrol prevents cognitive decline in SAMP8 mice. Curr Alzheimer Res 2017;14:820–33.
[12] Grimm MO, Lehmann J, Mett J, et al. Impact of vitamin D on amyloid precursor protein processing and amyloid-beta peptide degradation in Alzheimer's disease. Neurodegener Dis 2014;13:75–81.
[13] Vassar R, Bennett BD, Babu-Khan S, et al. Beta-secretase cleavage of Alzheimer's amyloid precursor protein by the transmembrane aspartic protease BACE. Science 1999;286:735–41.

[14] Hartmann T, Bieger SC, Bruhl B, et al. Distinct sites of intracellular production for Alzheimer's disease a beta 40/42 amyloid peptides. Nat Med 1997;3:1016–20.
[15] Sisodia SS. Beta-amyloid precursor protein cleavage by a membrane-bound protease. Proc Natl Acad Sci U S A 1992;89:6075–9.
[16] Crunkhorn S. Alzheimer disease: BACE1 inhibitor reduces beta-amyloid production in humans. Nat Rev Drug Discov 2016;16:18.
[17] Liu YG, Deng YY, Liu HY, Yin CX, Li XH, Gong QH. Hydrogen sulfide ameliorates learning memory impairment in APP/PS1 transgenic mice: a novel mechanism mediated by the activation of Nrf2. Pharmacol Biochem Behav 2016;150:207–16.
[18] Wang CY, Xie JW, Xu Y, et al. Trientine reduces BACE1 activity and mitigates amyloidosis via the AGE/RAGE/NF-kappa B pathway in a transgenic mouse model of Alzheimer's disease. Antioxid Redox Signal 2013;19:2024–39.
[19] Grimm MOW, Thiel A, Lauer AA, et al. Vitamin D and its analogues decrease amyloid-beta (Abeta) formation and increase Abeta-degradation. Int J Mol Sci 2017;18.
[20] Huse JT, Pijak DS, Leslie GJ, Lee VMY, Doms RW. Maturation and endosomal targeting of beta-site amyloid precursor protein-cleaving enzyme - the Alzheimer's disease beta-secretase. J Biol Chem 2000;275:33729–37.
[21] Kang EL, Biscaro B, Piazza F, Tesco G. BACE1 protein endocytosis and trafficking are differentially regulated by Ubiquitination at lysine 501 and the Di-leucine motif in the carboxyl terminus. J Biol Chem 2012;287:42867–80.
[22] Das U, Scott DA, Ganguly A, Koo EH, Tang Y, Roy S. Activity-induced convergence of APP and BACE-1 in acidic microdomains via an endocytosis-dependent pathway. Neuron 2013;79:447–60.
[23] Funmilayo E, Yeates A, Tesco G. The endosome-associated Deubiquitinating enzyme USP8 regulates BACE1 enzyme Ubiquitination and degradation. J Biol Chem 2016; 291:15753–66.
[24] Ye X, Cai Q. Snapin-mediated BACE1 retrograde transport is essential for its degradation in lysosomes and regulation of APP processing in neurons. Cell Rep 2014;6: 24–31.
[25] Cai QA, Lu L, Tian JH, Zhu YB, Qiao HF, Sheng ZH. Snapin-regulated late Endosomal transport is critical for efficient autophagy-Lysosomal function in neurons. Neuron 2010;68:73–86.
[26] Shibata M, Yamada S, Kumar SR, et al. Clearance of Alzheimer's amyloid-beta(1-40) peptide from brain by LDL receptor-related protein-1 at the blood-brain barrier. J Clin Investig 2000;106:1489–99.
[27] Storck SE, Meister S, Nahrath J, et al. Endothelial LRP1 transports amyloid-beta(1-42) across the blood-brain barrier. J Clin Investig 2016;126:123–36.
[28] Tanokashira D, Motoki K, Minegishi S, et al. LRP1 Downregulates the Alzheimer's beta-Secretase BACE1 by modulating its Intraneuronal trafficking(1,2,3). eNeuro 2015;2.
[29] Shah SA, Yoon GH, Chung SS, et al. Osmotin reduced amyloid beta (Abeta) burden by inhibiting SREBP2 expression in APP/PS1 mice. Mol Psychiatry 2017;22:323.
[30] Bengoechea-Alonso MT, Ericsson J. SREBP in signal transduction: cholesterol metabolism and beyond. Curr Opin Cell Biol 2007;19:215–22.
[31] Wang XX, Jiang T, Shen Y, et al. Vitamin D receptor agonist doxercalciferol modulates dietary fat-induced renal disease and renal lipid metabolism. Am J Physiol Ren Physiol 2011;300:F801–10.
[32] Dursun E, Gezen-Ak D. Vitamin D receptor is present on the neuronal plasma membrane and is co-localized with amyloid precursor protein, ADAM10 or Nicastrin. PLoS One 2017;12:e0188605.
[33] Dursun E, Gezen-Ak D, Yilmazer S. A novel perspective for Alzheimer's disease: vitamin D receptor suppression by amyloid-beta and preventing the amyloid-beta induced alterations by vitamin D in cortical neurons. J Alzheimers Dis 2011;23: 207–19.
[34] Eyles DW, Burne TH, McGrath JJ. Vitamin D, effects on brain development, adult brain function and the links between low levels of vitamin D and neuropsychiatric disease. Front Neuroendocrinol 2013;34:47–64.
[35] Sultana R, Perluigi M, Butterfield DA. Oxidatively modified proteins in Alzheimer's disease (AD), mild cognitive impairment and animal models of AD: role of Abeta in pathogenesis. Acta Neuropathol 2009;118:131–50.
[36] Shibutani S, Takeshita M, Grollman AP. Insertion of specific bases during DNA synthesis past the oxidation-damaged base 8-oxodG. Nature 1991;349:431–4.
[37] Kukreja L, Kujoth GC, Prolla TA, Van Leuven F, Vassar R. Increased mtDNA mutations with aging promotes amyloid accumulation and brain atrophy in the APP/Ld transgenic mouse model of Alzheimer's disease. Mol Neurodegener 2014;9:16.
[38] Santos RX, Correia SC, Zhu X, et al. Mitochondrial DNA oxidative damage and repair in aging and Alzheimer's disease. Antioxid Redox Signal 2013;18: 2444–57.
[39] de la Monte SM, Luong T, Neely TR, Robinson D, Wands JR. Mitochondrial DNA damage as a mechanism of cell loss in Alzheimer's disease. Lab Investig 2000;80: 1323–35.
[40] Oka S, Ohno M, Tsuchimoto D, Sakumi K, Furuichi M, Nakabeppu Y. Two distinct pathways of cell death triggered by oxidative damage to nuclear and mitochondrial DNAs. EMBO J 2008;27:421–32.
[41] Leon J, Sakumi K, Castillo E, Sheng Z, Oka S, Nakabeppu Y. 8-Oxoguanine accumulation in mitochondrial DNA causes mitochondrial dysfunction and impairs neuritogenesis in cultured adult mouse cortical neurons under oxidative conditions. Sci Rep 2016;6:22086.
[42] Sheng Z, Oka S, Tsuchimoto D, et al. 8-Oxoguanine causes neurodegeneration during MUTYH-mediated DNA base excision repair. J Clin Invest 2012;122:4344–61.
[43] Du J, Chen Y, Shi Y, et al. 1,25-Dihydroxyvitamin D protects intestinal epithelial barrier by regulating the myosin light chain kinase Signaling pathway. Inflamm Bowel Dis 2015;21:2495–506.
[44] Ronicke R, Mikhaylova M, Ronicke S, et al. Early neuronal dysfunction by amyloid beta oligomers depends on activation of NR2B-containing NMDA receptors. Neurobiol Aging 2011;32:2219–28.
[45] Opazo P, Viana da Silva S, Carta M, et al. CaMKII Metaplasticity drives Abeta oligomer-mediated Synaptotoxicity. Cell Rep 2018;23:3137–45.
[46] Sherman MA, Lesne SE. Detecting abeta*56 oligomers in brain tissues. Methods Mol Biol 2011;670:45–56.
[47] Lesne S, Koh MT, Kotilinek L, et al. A specific amyloid-beta protein assembly in the brain impairs memory. Nature 2006;440:352–7.
[48] Zhang S, Chai R, Yang YY, et al. Chronic diabetic states worsen Alzheimer neuropathology and cognitive deficits accompanying disruption of calcium signaling in leptin-deficient APP/PS1 mice. Oncotarget 2017;8:43617–34.
[49] Zafar S, Younas N, Correia S, et al. Strain-specific altered regulatory response of Rab7a and tau in Creutzfeldt-Jakob disease and Alzheimer's disease. Mol Neurobiol 2017;54:697–709.
[50] Laatsch A, Panteli M, Sornsakrin M, Hoffzimmer B, Grewal T, Heeren J. Low density lipoprotein receptor-related protein 1 dependent endosomal trapping and recycling of apolipoprotein E. PLoS One 2012;7:e29385.
[51] Sahara S, Yamashima T. Calpain-mediated Hsp70.1 cleavage in hippocampal CA1 neuronal death. Biochem Biophys Res Commun 2010;393:806–11.
[52] Annweiler C, Karras SN, Anagnostis P, Beauchet O. Vitamin D supplements: a novel therapeutic approach for Alzheimer patients. Front Pharmacol 2014;5:6.
[53] Littlejohns TJ, Henley WE, Lang IA, et al. Vitamin D and the risk of dementia and Alzheimer disease. Neurology 2014;83:920–8.
[54] Wang L, Hara K, Van Baaren JM, et al. Vitamin D receptor and Alzheimer's disease: a genetic and functional study. Neurobiol Aging 2012;33 [1844 e1841-1849].
[55] Gezen-Ak D, Atasoy IL, Candas E, Alaylioglu M, Yilmazer S, Dursun E. Vitamin D receptor regulates amyloid Beta 1-42 production with protein Disulfide Isomerase A3. ACS Chem Neurosci 2017;8:2335–46.
[56] Kummer MP, Schwarzenberger R, Sayah-Jeanne S, et al. Pan-PPAR modulation effectively protects APP/PS1 mice from amyloid deposition and cognitive deficits. Mol Neurobiol 2015;51:661–71.
[57] Yang W, Zhou K, Zhou Y, et al. Naringin Dihydrochalcone ameliorates cognitive deficits and neuropathology in APP/PS1 transgenic mice. Front Aging Neurosci 2018;10: 169.
[58] Lundgren JL, Ahmed S, Schedin-Weiss S, et al. ADAM10 and BACE1 are localized to synaptic vesicles. J Neurochem 2015;135:606–15.
[59] Brunholz S, Sisodia S, Lorenzo A, Deyts C, Kins S, Morfini G. Axonal transport of APP and the spatial regulation of APP cleavage and function in neuronal cells. Exp Brain Res 2012;217:353–64.
[60] Kizuka Y, Kitazume S, Fujinawa R, et al. An aberrant sugar modification of BACE1 blocks its lysosomal targeting in Alzheimer's disease. EMBO Mol Med 2015;7: 175–89.
[61] Wahle T, Prager K, Raffler N, Haass C, Famulok M, Walter J. GGA proteins regulate retrograde transport of BACE1 from endosomes to the trans-Golgi network. Mol Cell Neurosci 2005;29:453–61.
[62] von Einem B, Schwanzar D, Rehn F, et al. The role of low-density receptor-related protein 1 (LRP1) as a competitive substrate of the amyloid precursor protein (APP) for BACE1. Exp Neurol 2010;225:85–93.
[63] von Arnim CA, Kinoshita A, Peltan ID, et al. The low density lipoprotein receptor-related protein (LRP) is a novel beta-secretase (BACE1) substrate. J Biol Chem 2005;280:17777–85.
[64] Kanekiyo T, Cirrito JR, Liu CC, et al. Neuronal clearance of amyloid-beta by endocytic receptor LRP1. J Neurosci 2013;33:19276–83.
[65] Bell RD, Deane R, Chow N, et al. SRF and myocardin regulate LRP-mediated amyloid-beta clearance in brain vascular cells. Nat Cell Biol 2009;11:143–53.
[66] Asano L, Watanabe M, Ryoden Y, et al. Vitamin D metabolite, 25-Hydroxyvitamin D, regulates lipid metabolism by inducing degradation of SREBP/SCAP. Cell Chem Biol 2017;24:207–17.
[67] Li S, He Y, Lin S, et al. Increase of circulating cholesterol in vitamin D deficiency is linked to reduced vitamin D receptor activity via the Insig-2/SREBP-2 pathway. Mol Nutr Food Res 2016;60:798–809.
[68] Guo YX, He LY, Zhang M, Wang F, Liu F, Peng WX. 1,25-Dihydroxyvitamin D3 regulates expression of LRP1 and RAGE in vitro and in vivo, enhancing Abeta1-40 brain-to-blood efflux and peripheral uptake transport. Neuroscience 2016;322:28–38.
[69] Verghese PB, Castellano JM, Garai K, et al. ApoE influences amyloid-beta (Abeta) clearance despite minimal apoE/Abeta association in physiological conditions. Proc Natl Acad Sci U S A 2013;110:E1807–16.
[70] Seo J, Jo SA, Hwang S, et al. Trichostatin a epigenetically increases calpastatin expression and inhibits calpain activity and calcium-induced SH-SY5Y neuronal cell toxicity. FEBS J 2013;280:6691–701.
[71] Yamada KH, Kozlowski DA, Seidl SE, et al. Targeted gene inactivation of calpain-1 suppresses cortical degeneration due to traumatic brain injury and neuronal apoptosis induced by oxidative stress. J Biol Chem 2012;287:13182–93.
[72] Kurbatskaya K, Phillips EC, Croft CL, et al. Upregulation of calpain activity precedes tau phosphorylation and loss of synaptic proteins in Alzheimer's disease brain. Acta Neuropathol Commun 2016;4:34.
[73] Fa M, Zhang H, Staniszewski A, et al. Novel selective Calpain 1 inhibitors as potential therapeutics in Alzheimer's disease. J Alzheimers Dis 2016;49:707–21.